Eur. Phys. J. A (2024) 60:108
https://doi.org/10.1140/epja/s10050-024-01285-8

THE EUROPEAN PHYSICAL JOURNAL A

Review

Photons and nuclear structure

Norbert Pietralla[a]

Physics Department, Institute for Nuclear Physics, TU Darmstadt, Schlossgartenstrasse 9, 64289 Darmstadt, Germany

Received: 4 January 2023 / Accepted: 10 February 2024

Communicated by Calin Alexandru Ur

Abstract Beams of photons with energies ranging from a few hundred keV to a few tens of MeV have proven to be very usefull tools for studying a variety of nuclear structures and their properties. The peculiar features of photons allow for unique insights and precision. This contribution provides a collection of nuclear structure phenomena that are well accessible with photon beams and instructional examples for seminal experiments that have advanced nuclear structure research in the past using photons in the entrance channel. It is meant to complement the contents of other contributions highlighting the scientific and technological potential of the emerging field of *Nuclear Photonics*.

1 Introduction

Precise knowledge of the properties of atomic nuclei and their structural features are important ingredients for progress in many fields of science. One example is given by the broad field of nuclear astrophysics where particular resonances can dominate nuclear reaction rates that determine the stellar evolution or where the masses, structures, and lifetimes of heavy nuclei with extreme neutron excess may govern cosmic nucleosynthesis processes and thereby define the abundance pattern of matter in our World. Another example is given by metrology and detector technology in particle physics. Sophisticated neutrino detectors, for instance, require detailed knowledge on weak interaction processes on nuclei of their detection material for an accurate interpretation of the data. Many more examples for the scientific importance of nuclear structures stem from fields as diverse as medicine, material science, security, cosmology, and many others. Last, but no least, is the nuclear many-body system a fascinating research object by itself. Atomic nuclei represent the prime example for a multi-component, strongly coupled quantum system. It features an enormous richness of structures that arise from its two-component nature and from the competition between single-particle character and collectivity that reflect the shell structure of a mesoscopic quantum system. Some of the general structural features of such systems, like the Scissors Mode for example which occurs more generally in strongly-coupled, deformed, two-component quantum systems, have been first discovered in atomic nuclei.

Consequently, strong efforts are made to gain ever more detailed knowledge on nuclear structures, in particular, at the extremes of spin, isospin, temperature, and precision. International large-scale research facilities in Europe, such as FAIR or ELI-NP, are under construction for contributing to these efforts, and complementing those at several other laboratories world-wide, of which CERN, RIKEN, JLab, FRIB, or GANIL are some of the leading laboratories, all with distinct strengths and particular uniqueness. ELI-NP aims at contributing intense, narrow-bandwidth photon beams with energies between 1 and 20 MeV, ideally suited for nuclear structure research. MeV-ranged photons can provide unique information on the structure of atomic nuclei. On p.3 of their text book [1] Bohr and Mottelson write: *the study of nuclear transmutation by electromagnetic processes is an especially important tool for probing nuclear structure, because this interaction is relatively simple and has well-established properties.* Since photons have no rest mass, their impact on the nucleus induces little angular momentum, well suited for studying structures high above the yrast line, i.e. at comparatively high internal energy or temperature. Photons interact electromagnetically with the nucleus "at the photon point", i.e. the photonuclear reaction process can be fully separated without any ambiguity from the, potentially unknown, nuclear structure properties that, in turn, can then be measured to highest accuracy.

In memoriam of Professor Dr. Ulrich (Ulli) Kneissl, 24.3.1939–4.1.2023(†).

[a] e-mail: pietralla@ikp.tu-darmstadt.de (corresponding author)

Published online: 14 May 2024

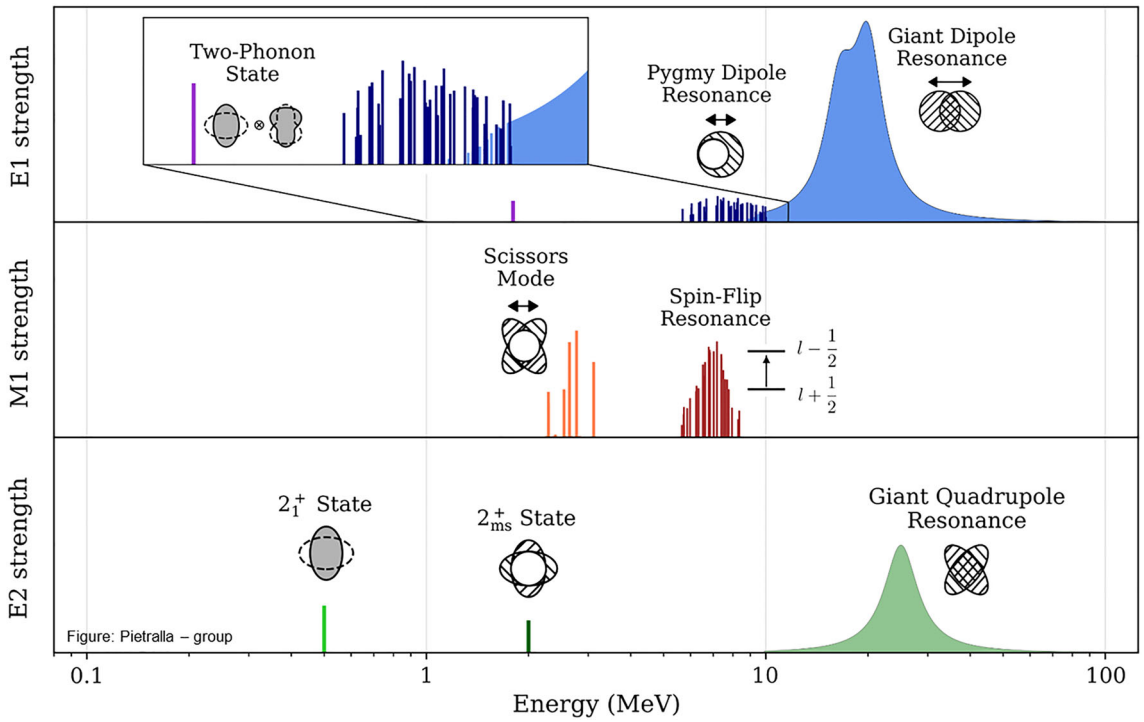

Fig. 1 Overview on nuclear structures that have been investigated by MeV-ranged photon beams and are discussed in this review

The constituents of the atomic nucleus, the nucleons, are composite particles, themselves. Their first excited state, the Δ resonance at 293 MeV excitation energy with isospin quantum number $T = 3/2$, decays electromagnetically to its $T = 1/2$ ground state, the nucleon N, with a branching ratio of 0.60(5)%. This isovector $M1$ transition features a partial decay width of $\Gamma_\gamma(\Delta) = 0.70(6)$ MeV with a strength of $B(M1; \Delta \rightarrow N) = 2.4(2)\mu_N^2$. It corresponds in the simple static quark model to a quark spin-flip which of course, can be induced as well by the absorption of a 293-MeV photon on the nucleus. Its reduced transition matrix element amounts to $|\langle \Delta \parallel M1 \parallel N \rangle| = 3.10(13)\mu_N$. Likewise, the simplest composite nucleus, the deuteron, can be excited from its stable $T = 0$, $J^\pi = 1^+$ ground state by an isovector $M1$ transition to the unbound $T = 1$, 0^+ resonance. This $M1$ transition, too, corresponds to a quark spin-flip, when the nucleons are naively modeled according to the static quark model. Its strength is difficult to determine experimentally because of the competing photodissociation channel of the deuteron above its binding energy of 2.225 MeV. The next simplest odd-odd nucleus beyond the deuteron is ^{6}Li. Its isovector $M1$ spin-flip excitation, the transition between the "quasideuteron states", the $T = 0$, 1^+ ground state and the $T = 1$, 0^+ state at 3.56 MeV, can be considered as resembling the situation in the deuteron. The reduced matrix element of this spin-flip transition has recently been studied in photon-induced reactions at the superconducting Darmstadt electron linear accelerator, S-DALINAC. It amounts to $|\langle 1^+_{T=0} \parallel M1 \parallel 0^+_{T=1} \rangle_{^6\mathrm{Li}}| = 3.95(4)\mu_N$, a value stunningly close to what is found for the quark spin-flip in the nucleon itself. The experiment and the fundamental interpretation of the data will be addressed in more detail in Sect. 3 below. At this point, I like to emphasize the precision of the value for the reduced transition strength of 1% which was possible to be obtained from photonuclear reactions for their clean electromagnetic character at the photon point. It is that precision which made the detailed interpretation of the data, the quantitative contribution of two-body currents to the given $M1$ transition matrix element, possible.

The literature offers a variety of excellent reviews on nuclear-structure research with photon beams. Most focus either on photonuclear reactions and their methodology, themselves, e.g. [2–9] or they provide overviews on the knowledge about certain nuclear structure phenomena as illustrated in Fig. 1, that were obtained, amongst other methods, by photonuclear reaction studies, e.g. [10–15]. I was invited to provide here an overview on examples for nuclear structure phenomena that can be approached and have been studied with photonuclear reactions with special emphasis on the particular strength that the usage of photon beams has contributed to the scientific advances. I restrict myself to the discussion of photonuclear studies of particle-bound structures in nuclei. Other phenomena will be addressed in other contributions to this booklet.

Since particle-bound nuclear structures can decay, only, internally by the emission of γ radiation, the corresponding

nuclear reactions induced by photon beams are restricted to (γ, γ') photon-scattering reactions. The corresponding reaction process is dominated by excited nuclear resonances and hence it is frequently dubbed Nuclear Resonance Fluorescence (NRF) in analogy to the optical phenomenon of absorption and fast re-emission of photons. The basic facts of the NRF method will be summarized in Sect. 2. The subsequent discussion of nuclear structures that had been studied with NRF will be grouped according to the dominant multipolarity of the excitation mode under discussion starting with magnetic dipole ($M1$) excitations. Next, I will discuss NRF studies of electric dipole ($E1$) modes and then conclude with the discussion of NRF research on electric quadrupole ($E2$) excitations. Monopole transitions cannot be induced by real photons[1] because of their finite helicity and magnetic quadrupole and higher multipole excitations typically have a too small transition probability such that their population in NRF reactions have not been observed and reported in the literature until now.

I hope that this contribution may be useful for students for a first overview on the powerfulness of photonuclear reactions for unambigous structural assignments of certain nuclear phenomena or that it may inspire them to tackle open questions exploiting MeV-ranged photon beams as nuclear probes. The latter goal might be served best by providing examples for successful nuclear structure studies. The present contribution is entirely based on previously published material, with only one exception. This contribution is dedicated to my teacher and colleague Ulli Kneissl who has passed away earlier this year. His seminal work on photonuclear reactions can serve us and the next generation of scientists as a rich source of experimental ingenuity and excellence. A dozen figures of his scientific legacy have been selected for illustrating the photonuclear approaches under discussion. Since I had been involved in some of the studies from that I have picked examples, I will occasionally use here exactly the same wording which I have previously found to express best the scientific situation in the original publications. This article does not aim at a full coverage of the literature. A largely complete set of reference citations to NRF studies on nuclei with atomic numbers ranging from 1 to 94 from the years between 2000 and 2020 can be found in Reference [9].

2 Nuclear resonance fluorescence

The resonant photon scattering reaction (γ, γ') which is often [2,4,5,9] referred to as Nuclear Resonance Fluorescence (NRF), is a two stage process. It represents the absorption of a real photon by an atomic nucleus exciting a nuclear resonance level at excitation energy E_r with spin and parity quantum numbers J^π and its subsequent internal deexcitation to lower-lying states by the emission of a photon. A schematic of the (γ, γ') reaction is sketched in Fig. 2. For its low momentum transfer the photon absorption primarily induces dipole excitations and to a lesser extent electric quadrupole excitations. The (γ, γ') reaction thus combines its spin selectivity with the strength sensitivity of an electromagnetic probe. NRF is ideally suited to study dipole excitations of stable nuclei. With photons in the exit channel, it can furthermore exploit the excellent energy resolution of γ-ray spectroscopy with Ge detectors. This allows for the identification of individual photoexcited states up to excitation energies for which the level density is rather high. Methods for integral measurements have been recently developed using quasi-monochromatic photon beams[2] that allow for accurate determination of average properties when the nuclear levels cannot be resolved anymore. An extensive review of the NRF method and its fundamental facts can be found in Ref. [9].

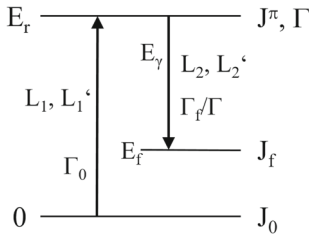

Fig. 2 Sketch of a nuclear level scheme relevant for an NRF reaction. A photon is absorbed on a ground state with spin quantum number J_0 thereby exciting the nucleus to a particle-bound level at excitation energy E_r with a cross section proportional to the partial ground state decay width Γ_0. The excited state with mean lifetime $\tau = \hbar/\Gamma$ subsequently decays with a branching ratio of Γ_f/Γ to a lower lying level J_f at excitation energy E_f by emitting a γ-ray with energy E_γ which will be detected. L_i and L_i' denote the leading and subleading multipolarities of the corresponding γ-ray transitions

Photoexcited states of different excitation energies can be investigated simultaneously if the incoming photons cover an appropriately wide energy range. This is the case for continuous-energy bremsstrahlung or, in pre-selected energy ranges, also for quasi-monochromatic photon beams from laser-Compton backscattering processes [7,9]. The observation of the resonantly scattered photons allows the extraction of numerous quantities from the data. The excitation energies E of the resonance states are obtained from the observed photon energies. At resonance energy the resonance scattering cross section is several orders of magnitude larger than any non-resonant process. Interference contributions from non-resonant processes can be neglected and the Breit-Wigner

[1] in contrast to virtual photons that do not need to satisfy the energy-momentum relation at the photon point.

[2] with typical band widths of a few %, like such provided by collimated laser-Compton backscattering, cf. [7,9].

resonance formula applies from which one can derive the energy integrated cross section ($d\sigma/d\Omega$) for the photoinduced resonance excitation at resonance energy E_r and its decay to a final state J_f and photon emission into the solid angle element $d\Omega$.

The energy-integrated photon-scattering cross section for an isolated resonance state is given [9] by

$$\left(\frac{d\sigma}{d\Omega}\right)(\vartheta,\phi) = g\left(\frac{\pi\hbar c}{E_r}\right)^2 \Gamma_0 \frac{\Gamma_f}{\Gamma}\frac{W(\vartheta,\phi)}{4\pi} = I_{s,f}\frac{W(\vartheta,\phi)}{4\pi} = \frac{(A/\epsilon)(\vartheta,\phi)}{\mathcal{L}}. \quad (1)$$

Here $\Gamma = \Gamma_0 + \sum_{f>0}\Gamma_f$ denotes the total level width while Γ_0 (Γ_f) denote the partial decay widths to the ground state (to the fth excited state) and $g = (2J+1)/(2J_0+1)$ is the "spin factor". J_0 and J are the spins of the ground state and of the resonance state, respectively. $W(\vartheta,\phi)$ represents the normalized angular distribution function of the photon-scattering intensity relative to the direction of the incident photon beam (polar angle ϑ) and eventually to its polarization plane (azimuthal angle ϕ). The total, energy and solid angle integrated, cross section for the exclusive resonance scattering reaction into the final channel f is denoted by $I_{s,f}$. The counts at observation angles $A(\vartheta,\phi)$ equal the product of cross section and experimental luminosity times the detection efficiency $\epsilon(\vartheta,\phi)$ at these angles. The luminosity $\mathcal{L} = \Phi_\gamma(E_r)\,\bar{n}_t\,T$ is given by the product of the photon flux at resonance energy, target areal number density, and measuring time. Despite of the minimal momentum transfer of photons, the energy mismatch between a photon issued by a nucleus at rest decaying from an excited state at MeV-scale excitation energy to the ground state and a photon capable of exciting the nucleus at rest from the ground state is, due to the finite nuclear recoil of the order of E_γ/Mc^2, larger than the natural line width Γ of the excited state.

The spin and parity quantum numbers J^π of the excited states as well as the leading and subleading multipolarities of the photon excitation reaction can be determined from the angular distribution of the γ-decay transition of the resonance state to the ground state about the direction of the incident photon beam and its polarization plane. In general, this may require a very high statistical accuracy. In the favorable case of NRF of even–even nuclei with 0^+ ground states induced by a fully polarized incident photon beam, the determination of the spin quantum number, $J = 1$ or $J = 2$, of the photoexcited state and its parity quantum number π is comparably easy because the different angular distribution patterns are very pronounced and several dozens of counts under well selected observation angles may already suffice for unambiguous assignments of spin and parity quantum numbers [9,16–19]. In the peculiar situation of excited states of odd-mass nuclei with $J = 1/2$ spin quantum number, a measurement of its parity is not possible [20].

The photo-excited states may not only decay back to the ground state but also to excited states. The ratio Γ_f/Γ_0 of partial decay widths to the fth excited state relative to the ground state is determined from the relative decay intensities and from the knowledge of the spins and transition multipolarities involved using the relation

$$\frac{\left(\frac{d\sigma}{d\Omega}\right)_f(\vartheta,\phi)}{\left(\frac{d\sigma}{d\Omega}\right)_0(\vartheta,\phi)} = \frac{\Gamma_f}{\Gamma_0}\frac{W_{J_0JJ_f}(\vartheta,\phi)}{W_{J_0JJ_0}(\vartheta,\phi)} = \left.\frac{A/\epsilon(E_{\gamma_f})}{A/\epsilon(E_{\gamma_0})}\right|_{\vartheta,\phi} \quad (2)$$

For dipole excitations of even–even nuclei with spin quantum number $J = 1$, the strong decay branches are of dipole character, too, and they populate low-lying states with $J_f = 0$ and $J_f = 2$. For $J_f = 2$ the transition $J = 1 \to J_f = 2$ may consist of mixed multipolarity. A list of angular distribution functions $W_{J_0JJ_f}(\vartheta,\phi)$ for NRF intensities for an exhaustive variety of relevant spin sequences is tabulated and provided in appendix A of Ref. [9]. The angular distribution function for NRF intensity for the ground-state decay of a dipole-excited $J = 1$ state of an even–even nucleus with parity π_x, i.e., with a $0^+ \xrightarrow{\vec{\gamma}} 1^{\pi_x} \xrightarrow{\gamma} 0^+$ spin cascade, about a linear-polarized incident photon beam with degree of polarization P_γ is given, for example, by the expression

$$W_{0^+-1^{\pi_x}-0^+}(\vartheta,\phi) = \frac{3}{4}\left[1 + \cos^2(\vartheta) + \pi_x P_\gamma \cos(2\phi)\sin^2(\vartheta)\right]. \quad (3)$$

The interpretation of nuclear structures generating pronounced NRF signals requires information on their parity quantum numbers. Assignments of parity quantum numbers from NRF can be based on the polarization of at least one of the γ quanta involved. Either a polarized photon beam must be used in the entrance channel or polarization must be measured in the exit channel. The latter was frequently done, see, e.g. Refs. [5,6], using Compton polarimeters until the advent of intense polarized MeV-range photon beams from LCB processes. However, Compton polarimetry is difficult at γ-energies exceeding 4 MeV because the analyzing power of the Compton scattering process is energy dependent and becomes prohibitively small at these energies.

Using polarized photons in the entrance channel and measuring the intensity distribution with respect to the polarization plane of the beam is preferable for parity measurements in NRF experiments. In many important cases, such as ground-state decay transitions of $J = 1$ states of even–even nuclei, the angular distribution function of which is given in Eq. (3), the analyzing power of this process is 100% and independent of the energy of the γ-ray transition. Therefore, already modest counting statistics with peak areas A can suffice to make parity assignments in these cases, and in addition the measurement of NRF intensity is comparatively simple as shown in Fig. 3. This method has mostly been

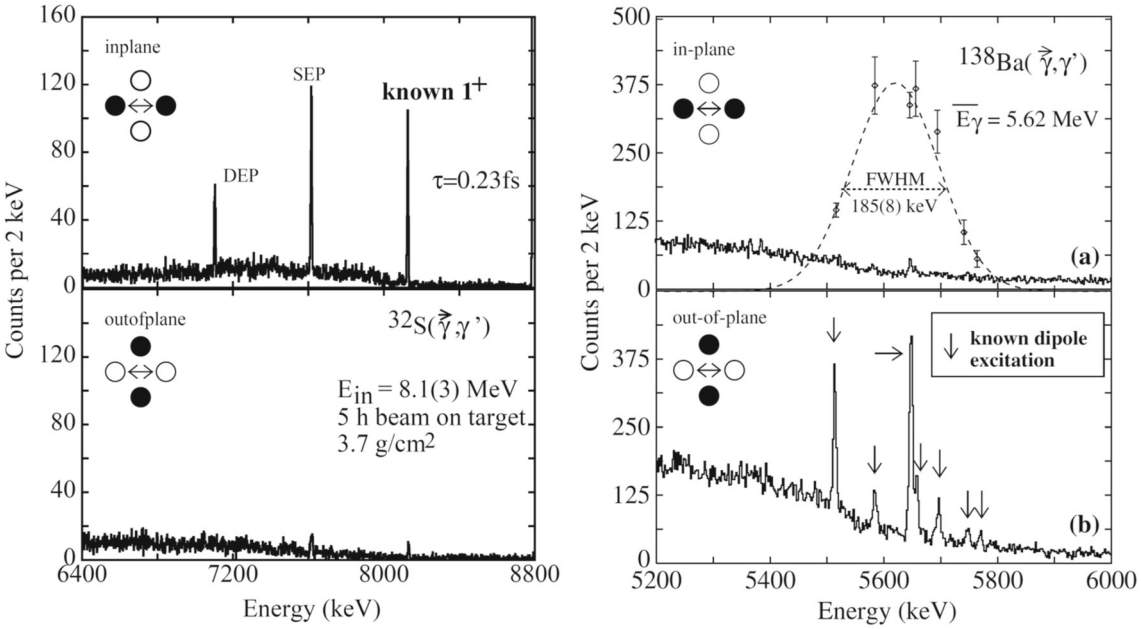

Fig. 3 (*Left:*) NRF intensities scattered off a sample of natural sulfur irradiated with a nearly monochromatic γ-ray beam with energy 8.125 MeV at the High-Intensity γ-ray Source (HIγS) observed at a polar angle $\vartheta = 90°$ in the polarization plane of the incident γ-ray beam (top) and perpendicular to it (bottom). The high NRF intensity asymmetry observed for the 8.124 MeV $1^+ \rightarrow 0_1^+$ $M1$ transition in ^{32}S demonstrates the polarization sensitivity of the TUNL/HIγS-polarimeter. *Reprinted from Ref.* [17], *©(2002), with permission from Elsevier*. (*Right:*) Photon scattering spectra obtained using a $BaNO_3$ target in the same set-up as described above. The arrows mark known dipole excitations of ^{138}Ba with previously uncertain parity quantum numbers. The few-hours long NRF measurement with the polarized photon beam of the HIγS facility was sufficient for making unambigous $J^\pi = 1^-$ spin/parity assignments to all of them. The dashed curve in (a) is a Gaussian with FWHM 185(8) keV indicating the spectral shape of the incident photon beam. *Reprinted with permission from Ref.* [16], *©(2002), by the American Physical Society*

applied for polarimetry in NRF measurements since about the turn of the century [16–18]. Off-axis bremsstrahlung can provide partially-polarized photon beams that have been and are still used at some facilities, e.g., γELBE at the Helmholtz-Zentrum Dresden-Rossendorf (HZDR). The following formulation is applicable also in those cases. A recent overview on MeV-ranged photon sources is provided in Ref. [9].

The analyzing power of the $0^+ \xrightarrow{\vec{\gamma}} 1^{\pi_x} \xrightarrow{\gamma} 0^+$ NRF cascade is given by

$$\Sigma = \frac{W(90°,0°) - W(90°,90°)}{W(90°,0°) + W(90°,90°)} = \pi_x = \begin{cases} +1 \text{ for } J^\pi = 1^+ \\ -1 \text{ for } J^\pi = 1^- \end{cases} . \tag{4}$$

For a partially polarized beam with $P_\gamma < 1$, as for instance provided by off-axis bremsstrahlung, the experimental asymmetry is reduced proportional to P_γ. An experimental setup with a finite polarization sensitivity $Q \leq 1$, e.g., due to finite opening angles of detectors, and with an intrinsic instrumental asymmetry a, is capable of detecting the polarization asymmetry

$$\epsilon = \frac{A(90°,0°) - aA(90°,90°)}{A(90°,0°) + aA(90°,90°)} = Q P_\gamma \Sigma \in [-1,1] . \tag{5}$$

Instrumental asymmetries a can be calibrated by using unpolarized or fully circularly-polarized photon beams for which the RHS of Eq. (5) vanishes. Then, the polarization sensitivity Q needs to be calibrated on a signal with a known analyzing power, e.g. as defined in Eq. (4). In contrast to Compton polarimeters, the polarization sensitivity of an intensity measurement about a fully polarized photon beam can be close to 100% independently of the γ-ray energy. NRF polarimetry about a fully-polarized photon beam can, therefore, be a very sensitive method for the assignment of the polarity of a given γ-ray transition and, hence, of parity quantum numbers of photoexcited nuclear levels of interest. Its figure-of-merit, usually defined as the absolute detection efficiency times the square of the polarization sensitivity of the setup, can be three orders of magnitude larger than for Compton polarimetry, reducing the necessary measurement time from a few weeks [5] to a few hours [18].

Besides the spin and parity quantum numbers of the involved nuclear states, the NRF angular distributions and asymmetries depend in general on possible multipole mixing ratios for the involved populating and depopulating transitions. In the relevant situation of leading $M1$ and subleading $E2$ multipolarities, the $E2/M1$ multipole mixing ratio δ is

defined in the phase convention of Ref. [21] as

$$\delta = \frac{\langle \Psi_f \parallel j_N A_2^E \parallel \Psi_i \rangle}{\langle \Psi_f \parallel j_N A_1^M \parallel \Psi_i \rangle} = \frac{\sqrt{3}}{10} \frac{E_\gamma}{\hbar c} \frac{\langle \Psi_f \parallel E2 \parallel \Psi_i \rangle_{\mathrm{BM}}}{\langle \Psi_f \parallel M1 \parallel \Psi_i \rangle_{\mathrm{BM}}} \tag{6}$$

The second equation in (6) gives the relation of the $E2/M1$ mixing ratio to the reduced matrix elements of the transition operators as defined by Bohr and Mottelson [1]. Since the NRF angular distribution functions $W(\vartheta, \phi)$ in general depend on the multipole mixing ratios, they can be used to measure subdominant multipole components to the studied NRF γ-ray transitions [22].

From the ratio of partial decay widths Γ_1/Γ_0 and the corresponding multipole mixing ratio δ of $1^\pi \rightarrow 2^+$ transitions, e.g. for the decays to the ground state band of a deformed nucleus, one can form the branching ratio

$$R_{\mathrm{expt}} = \frac{\Gamma_1/E_{\gamma 1}^3}{\Gamma_0/E_{\gamma 0}^3} = (1+\delta^2) \frac{B(\Pi 1; 1^\pi \rightarrow 2_1^+)}{B(\Pi 1; 1^\pi \rightarrow 0^+)} \tag{7}$$

where E_γ is the energy of the corresponding γ-ray transition. Such branching ratios have a particular significance for axially symmetric, deformed nuclei for which they can be related to the intrinsic projection quantum number K. The ratio of the transition strengths to a lower-lying band on the RHS of (7) can be calculated from the Alaga rule [23] for ideal axially symmetric rotors where the states have a good K quantum number. It simply depends on the squared ratio of Clebsch-Gordan coefficients. The ratio of the dipole transition strengths to the $K = 0$ ground state band, for example, is hence estimated by

$$R_{\mathrm{Alaga}} = \frac{B(\Pi 1; 1_K^\pi \rightarrow 2^+_{1,K_f=0})}{B(\Pi 1; 1_K^\pi \rightarrow 0^+_{1,K_f=0})} = \left(\frac{C^{2\,0}_{1\,K\,1\,\Delta K}}{C^{0\,0}_{1\,K\,1\,\Delta K}} \right)^2 = \begin{cases} 2.0 \\ 0.5 \end{cases} \text{for} \begin{matrix} K=0 \\ K=1 \end{matrix} \tag{8}$$

such that a K quantum number can often be assigned with sufficient sensitivity.

NRF experiments make measurements of absolute values for the photon scattering cross sections in Eq. (1) possible by a determination of the experimental detection efficiencies and luminosity. The latter can be obtained relative to a photon flux calibration target for a set of energies for which levels with sufficiently well known NRF cross sections are available. This procedure is much easier for photon beams with a weak energy-dependence of the photon intensity, such as bremsstrahlung, than for photon sources with narrow bandwidth. The observed cross sections of the nucleus under investigation are then compared to the well known cross sections of the calibration standard that is simultaneously irradiated by the photon beam. This makes the accurate measurement of NRF cross sections with bremsstrahlung beams often easier as compared to quasi-monochromatic photon beams that instead offer higher sensitivities and lower background. Ideally, data from NRF experiments using bremsstrahlung and quasi-monochromatic photon sources can be combined to allow for highest possible sensitivity and accuracy for NRF cross sections. A powerful alternative is provided by the nuclear self-absorption method as shown, e.g., in Sect. 3.1.1 below.

From the cross section for the elastic scattering process $(d\sigma/d\Omega)_0$ from (1) one obtains the quantity $\Gamma_0 \cdot \Gamma_0/\Gamma$. The relative ground state decay width $\Gamma_0/\Gamma = 1/(1 + \sum_{f>0} \Gamma_f/\Gamma_0)$ can be determined from the observed decay branching ratios provided no significant branches go undetected. This condition can better be met by using quasi-monochromatic beams with low background and high sensitivity even to weak decay branches or to the effective internal population of low-energy levels. Thus absolute values for the ground state decay widths Γ_0 and for the total level widths Γ can be extracted from the experiment. Level lifetimes can then be obtained from the relation $\tau = \hbar/\Gamma$.

The partial decay widths

$$\Gamma_f = 8\pi \sum_{\Pi\lambda}^{J+J_f} \frac{\lambda+1}{\lambda[(2\lambda+1)!!]^2} \left(\frac{E_\gamma}{\hbar c} \right)^{2\lambda+1} B(\Pi\lambda; J \rightarrow J_f) \tag{9}$$

provide the reduced transition strengths if the transition is dominated by a single multipole or if the multipole mixing ratios are known. The excitation of an even–even nucleus with a $J_f^\pi = 0^+$ ground state proceeds with the pure multipole $\lambda = J$. It is apparent from (9) that the dipole excitation strength

$$B(\Pi 1)\uparrow = g B(\Pi 1; 1^\pi \rightarrow 0^+) = \frac{27}{16\pi} \frac{\Gamma_0}{(E_\gamma/\hbar c)^3} \tag{10}$$

can be deduced from the photon scattering experiment in units of keV fm^3 without the knowledge of the parity of the dipole excitation. Usually dipole strengths are expressed in terms of nuclear magnetons ($\mu_N = e\hbar c/2m_p c^2$) for $M1$ transitions or in terms of $10^{-3}\, e^2\mathrm{fm}^2$ for $E1$ transitions. With the numerical value $\hbar c \approx 197.33$ MeV fm, the fine structure constant $\alpha = e^2/\hbar c \approx 1/137$ and, hence $e^2 \approx 1.44$ MeV fm, these units are connected by the relation

$$1\ \mu_N^2 = 11.06 \times 10^{-3}\, e^2\mathrm{fm}^2 = 15.9\ \mathrm{keV\,fm}^3\ . \tag{11}$$

The observables of a photon scattering experiment - the γ-ray energies and angular-dependent scattering intensities -

provide precious spectroscopic quantities, depending on the details of the chosen setup. They include

- γ-ray transition energies E_γ and their placements in the nuclear level scheme
- level energies E_x
- multipolarities $\Pi\lambda$ of γ-ray transitions
- spin quantum numbers J of nuclear levels
- parity quantum numbers π of nuclear levels
- multipole-mixing ratios δ of γ-ray transitions
- γ-decay branching ratios Γ_f / Γ_i
- K-quantum numbers of axially deformed nuclear levels
- integrated photonuclear resonance cross sections $I_{s,f}$
- monopolar partial decay widths $\Gamma_{f,\Pi\lambda}$
- total level widths Γ
- level lifetimes τ
- ground state excitation strengths $B(\Pi L; \text{gs} \rightarrow J^\pi)$
- decay transition strengths $B(\Pi L; J^\pi \rightarrow J_f^{\pi_f})$.

The next section will address examples for nuclear structures that have been successfully studied with NRF experiments.

3 Selected examples for nuclear structures studied by NRF

This section provides on overview on the impact of NRF measurements on low-spin nuclear structure physics. The examples are grouped according to their dominant multipolarity. Examples of pronounced $M1$ excitations are discussed first, followed by selected low-energy $E1$ and $E2$ structures.

3.1 $M1$ excitations

The $M1$ transition operator

$$T(M1) = \frac{3}{4\pi}\left[\sum_Z (g_l^p \hat{l}_p + g_s^p \hat{s}_p) + \sum_N (g_l^n \hat{l}_n + g_s^n \hat{s}_n)\right]\mu_N \tag{12}$$

$$= \frac{3}{4\pi}\left[\sum_A g_l^{\text{IS}} \hat{l} + \frac{g_s^{\text{IS}}}{2}\hat{\sigma} - \left(g_l^{\text{IV}} \hat{l} + \frac{g_s^{\text{IV}}}{2}\hat{\sigma}\right)\hat{\tau}_0\right]\mu_N \tag{13}$$

contains spin ($\hat{s}$) and orbital ($\hat{l}$) contributions for protons and neutrons with their corresponding gyromagnetic factors (g) and can be decomposed in the isoscalar (IS) and isovector (IV) parts. Since the neutron is uncharged, it has a negative spin-g factor, and the free isovector spin g-factor, $g_s^{\text{IV}} = +4.7$ is larger than the other three g-factors by a factor five to ten. Nuclear $M1$ excitations can therefore be expected to be dominated by their spin-isospin component. This is often the case, indeed, in particular for comparatively light nuclei where shell model orbitals with large angular momentum quantum numbers are not occupied. For heavier nuclei or when nuclei deform, rotations become important and orbital contributions to the $M1$ strength can increase. NRF experiments have contributed tremendously to the clarification of the corresponding nuclear structures. We will discuss here examples for NRF studies of structures that are considered to be either dominated by the spin-isospin part of the $M1$ operator or to be due to orbital character.

3.1.1 *Isovector $M1$ excitation of ^{6}Li*

As it was mentioned already in the Introduction above, $M1$ transitions between quasi-deuteron configurations of odd-odd $N = Z$ nuclei with isospin quantum numbers $T = 0$ and $T = 1$ can belong to the strongest $M1$ transitions to be found in the nuclear chart, provided that they are formed by spin-aligned single-particle orbitals with spin quantum numbers $j = l + 1/2$ [24]. Of particular importance is the decay transition of the excited 0^+ state of ^{6}Li at an excitation energy of 3.56 MeV with isospin $T = 1$ to its 1^+ ground with $T = 0$. This transition represents the "first γ-ray transition in the nuclear chart" in the sense that the 0_1^+ state of ^{6}Li is the lightest non-strange nuclear system which predominantly decays by electromagnetic radiation. It is, therefore, a very appealing object for theoretical studies, too.

Advanced, no-core shell-model calculations using effective nucleon-nucleon forces derived from chiral effective field theory (χEFT) require the consideration of two-body currents in the description of transition operators. Sensitive tests of the adequate modelling call for high precision and accuracy of the data on transition strength. Direct measurements of the decay rate of the 0_1^+ state of ^{6}Li with its short halflife of less than 60 as are impossible. The $B(M1; 0^+ \rightarrow 1_{\text{gs}}^+)$ value was recently remeasured [25] to a precision of about 2% by the recently developed Relative Self-Absorption (RSA) method, a sensitive variant of NRF. Previous data were either not precise enough or they were based on extrapolations of reaction theory such that a remeasurement with sufficient precision directly at the photon point had been desirable.

NRF of a mixed $^6Li_2CO_3/^{11}B$ sample has been studied at the bremsstrahlung site of the S-DALINAC at Darmstadt [25]. In one part of the experiment, the incident photon flux was modified by an absorber containing ^{6}Li, such that photons at resonance energy were absorbed and removed from the beam which was incident on the NRF target. The corresponding reduction of the NRF count rate is a direct measure for the NRF cross section once the attenuation of the beam by atomic processes on the absorber material had been removed. This was done by normalization of the NRF signals from ^{11}B nuclei that were present in the NRF target. The data are dis-

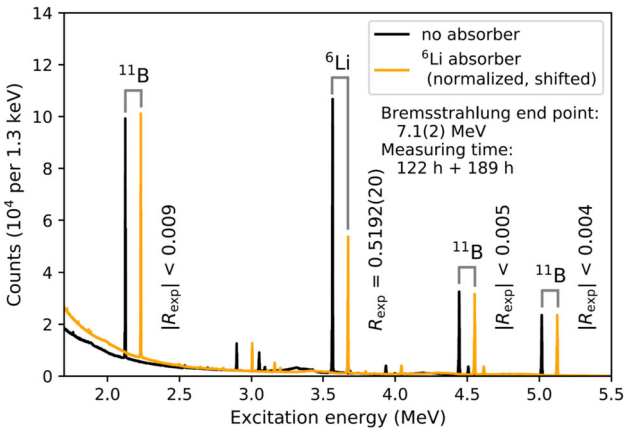

Fig. 4 Self-absorption measurement of the $M1$ decay strength of the 0_1^+ state of ^{6}Li at 3.56 MeV excitation energy. The figure shows two NRF spectra, one of which is shifted by 100 keV for better visibility. That one was obtained by having modified the incident bremsstrahlung beam with a resonant absorber and normalized to NRF lines from ^{11}B nuclei that were present in the NRF target but absent in the absorber. A self-absorption effect could be measured to a precision of a few tenth of a percent. *Reprinted with permission from Ref.* [25], *©(2021), by the American Physical Society*

played in Fig. 4. The measured amount of self-absorption resulted in a precise measurement of the $M1$ transition strength with a value of $B(M1; 0_1^+ \rightarrow 1_{gs}^+) = 15.61(33)\mu_N^2$ which confirmed the most precise measurement from electron scattering, this time, however, from an experiment performed directly at the photon point. The data support the necessity of the consideration of two-body currents for a modeling of electromagnetic transitions at this level of accuracy [25].

3.1.2 *Spin-flip strength in ^{40}Ar*

As mentioned above, detailed knowledge of particular nuclear structures are of paramount importance for detector technology in particle and astroparticle physics. Large-scale efforts address the characterization of neutrino properties and cosmic neutrino sources. As a scintillation detector material for weak processes, liquid argon has several advantages over other materials due to its chemical and physical properties, for example, its noblegas character and comparably high density. The case of LAr is, moreover, advantageous because the isotope ^{40}Ar has a very high natural abundance of 99.6% which makes the element practically monoisotopic and the detector response easy to interprete once the response of ^{40}Ar is fully understood. Consequently, liquid-argon time-projection chambers (LAr-TPCs) are uti-

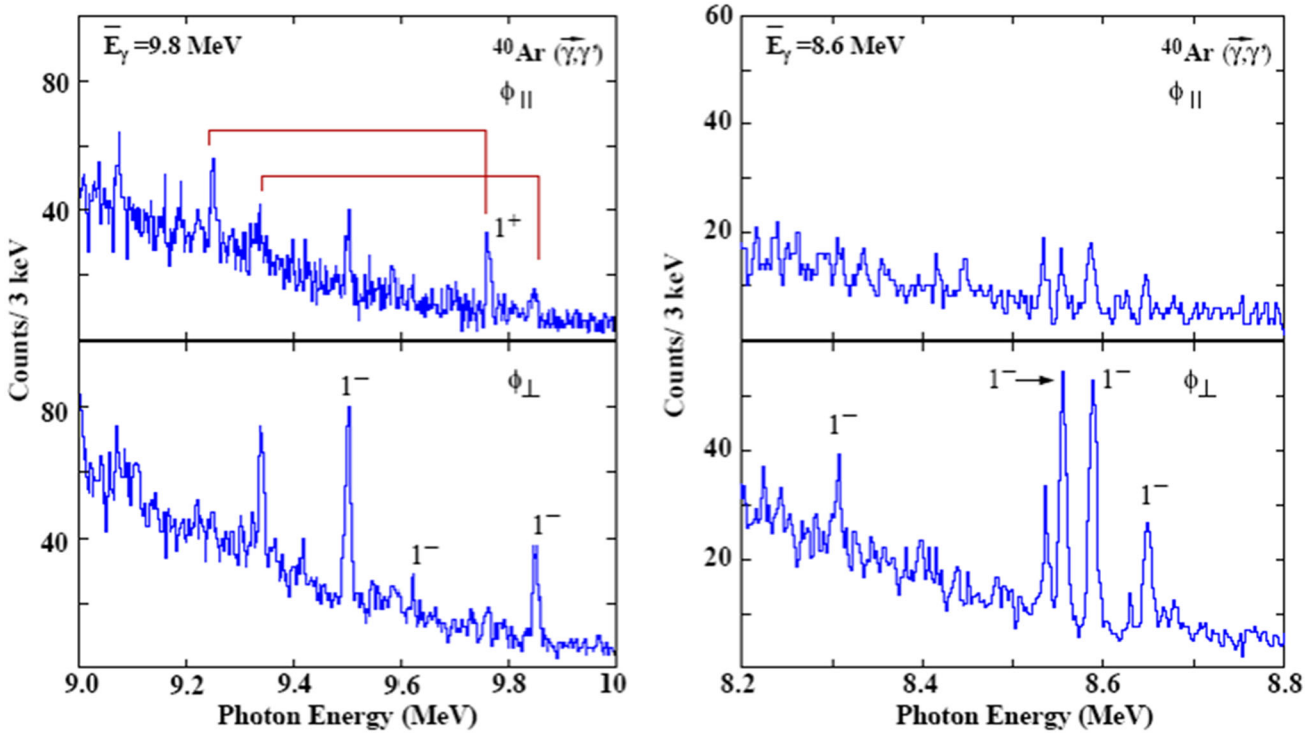

Fig. 5 Spectra of the ^{40}Ar$(\vec{\gamma}, \gamma')$ reaction at HIγS. Data were taken at a polar angle $\vartheta = 90°$ relative to the incident photon beam and azimuthal angles $\phi_\parallel$ (top) and $\phi_\perp$ (bottom) relative to the polarization plane of the γ-ray beam. The mean γ-ray energy of the incident beam is given in the upper left corners. The J^π assignments are indicated for the ground state transitions in ^{40}Ar. Some single escape peaks are indicated by red brackets. *Reprinted with permission from Ref.* [26], *©(2006), by the American Physical Society*

lized for neutrino detection for example DUNE, the Deep Underground Neutrino Experiment, at the Sanford Underground Research Facility (SURF) in South Dakota. As weak interaction processes proceed predominantly via the $\sigma\tau$ spin-isospin operator, the neutral-current neutrino interactions is closely related to the spin-part of the $M1$ operator from Eq. (13).

Magnetic dipole excitations of ^{40}Ar had been unknown until Li et al. [26] announced in 2006 the first observation of a 1^+ state of ^{40}Ar in data from an NRF study at the High Intensity γ-ray Source (HIγS) at Duke University. The data are displayed in Fig. 5. Subsequent NRF experiments by Gayer et al. [27] and by Tornow et al. [28] have more than tripled the $M1$ excitation strength known for ^{40}Ar. The latter study provided clear evidence for seven additional 1^+ states of ^{40}Ar including a $1^+/1^-$ parity doublet near 9.85 MeV which had been visible already in the earlier data by Li et al. (see the lower red bracket in the top left panel of Fig. 5) although inconclusive at the time because of insufficient counting statistics for a clean disentanglement of the doublet.

The close relationship between the spin-isovector component of the $M1$ and the Gamow-Teller transition probabilities was used by Tornow et al. [28] to calculate the neutral current neutrino and antineutrino cross sections for reactions with ^{40}Ar. They predicted cross sections based on shell-model calculations that were scaled to reproduce their measured $M1$ strengths and 1^+ excitation energies. The leading-order approximation was found to be accurate for neutrinos at low supernova energies (up to about 20–30 MeV). The inclusion of operators at all-orders in momentum transfer was found to suppress both and to distinguish between the neutrino and antineutrino cross sections above 20 MeV [28].

3.1.3 Scissors Mode

The scissors mode (ScM) is a collective orbital $M1$ excitation of deformed, coupled, two-fluid quantum systems, in which the two deformed sub-systems can exhibit counter-rotational out-of-phase oscillations against each other in a scissors-like fashion. It can occur in a variety of quantum systems [14, and references therein]. In nuclei it is characterized by a comparatively strong $M1$ excitation from the ground state. In even–even nuclei the ScM is carried by excited states with spin and parity quantum numbers $J^\pi = 1^+$ and intrinsic projection quantum number $K = 1$.

The ScM has first been observed experimentally in deformed nuclei in the mid-1980s using inelastic electron-scattering reactions on the nuclide ^{156}Gd [29]. An accumulation of weakly fragmented $M1$ excitation strength was associated with the nuclear ScM. Its discovery by the group of Richter has historically led to a renaissance of experimental activities employing photonuclear reactions on bound nuclear states at comparatively low-excitation energies of about 2–5 MeV by the groups of Kneissl, von Brentano, and Richter. The NRF technique can be advantageous over other experimental approaches to the nuclear ScM in terms of energy resolution, sensitivity, and access to decay properties [30]. Figure 6 shows a comparison between NRF and electron scattering for the study of the ScM.

Extensive reviews have been published [4,5,10–12,14] on the nuclear ScM until about a decade ago. The investigation of the ScM using NRF has recently advanced, in particular by employing the opportunities offered by the advent of intense, quasi-monochromatic, fully polarized photon beams from LCB sources. Examples of these developments are compiled in this subsection along with classical studies using intense bremsstrahlung.

Evidence and fragmentation

Low-energy $M1$ excitations have been studied by the NRF technique in dozens of deformed nuclei. Since its discovery in ^{156}Gd (see above) the initial NRF studies of the ScM were focused on deformed even–even nuclei in the Rare Earth mass region and the Actinides. Figure 7 shows the data on the initial observation of the ScM in even–even nuclei of the Dysprosium isotopic chain by Wesselborg et al. [32]. The ScM appears as a somewhat fragmented distribution of $M1$ strength localized in a certain energy range of a few hundred keV width.

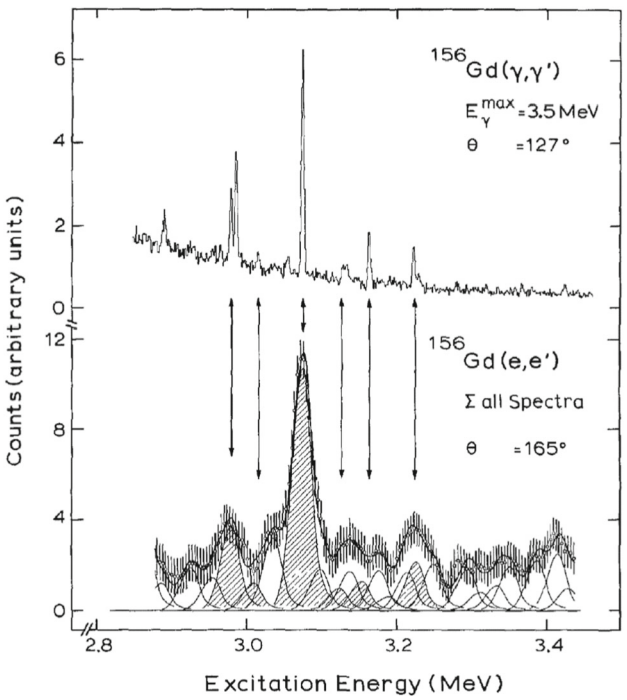

Fig. 6 Spectra of the ^{156}Gd(γ, γ') reaction using bremsstrahlung at the Stuttgart DYNAMITRON accelerator and from electron scattering providing evidence for the scissors mode. The NRF data provide better energy resolution and sensitivity to decay transitions to excited states. *Reprinted from Ref.* [31], *©(1986), with permission from Elsevier*

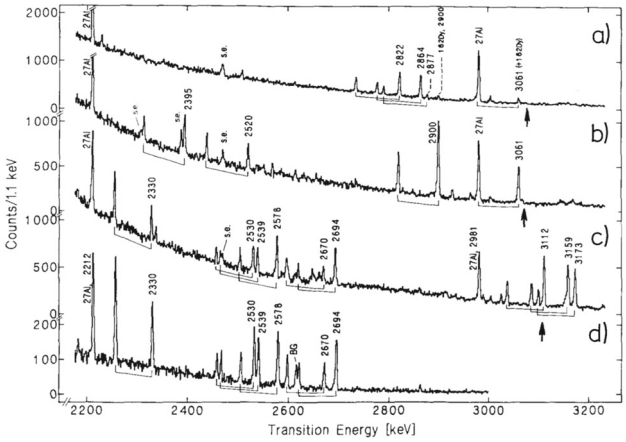

Fig. 7 NRF-spectra of ^{160,162,164}Dy (labelled **a**–**c**, respectively) measured with 4.1 MeV, and of ^{164}Dy, (d), measured with 2.9 MeV bremsstrahlung endpoint energy at 130° to the incoming γ-beam. No background has been subtracted. Energies of g.s. transitions are given in keV. Brackets below the peaks indicate corresponding transitions to the 2_1^+ state. Spectra **a**–**c** have been normalized to the 2981-keV transition in ^{27}Al, which was used to calibrate the photon flux. In **d**, due to the lower endpoint energy, the peak-to-back-ground ratio at 2.6 MeV has been increased by roughly a factor of four and all single escape lines from transitions around 3 MeV have disappeared. *Reprinted from Ref.* [32], *©(1988), with permission from Elsevier*

Spin quantum numbers $J = 1$ had unambigously been measured from polar angular distributions of the NRF intensities. Decay branching ratios to the ground state and the 2_1^+ state, respectively, had been used to assign K-quantum numbers $K = 1$ to the fragments of the ScM in the cases of deformed nuclei. The assignment of parity quantum numbers to the nuclear dipole excitations observed between 2 and 5 MeV in NRF experiments had not been so straightforward in the end of the last century when intense, fully polarized beams of MeV-ranged photons were still lacking. In a few cases, parity information had been available either from complementary experiments, such as electron-scattering, particle-scattering or studies of β-decay reactions, or from γ-ray Compton polarimetry in NRF experiments themselves. The latter had sensitivities of a few percent and were applicable to the strongest dipole excitations, only, because they required a large amount of beam time. Compton polarimetry in NRF experiments on the ScM had been performed by Kasten et al. on ^{150}Nd [33], Heil et al. on ^{142,150}Nd and ^{232}Th [34], Friedrich et al. on ^{150}Nd, ^{162}Dy [35] and on ^{160}Gd [36], Margraf et al. on ^{146}Nd [37] and on ^{162,164}Dy [38], Maser et al. on ^{134}Ba [39] and on ^{168}Er [40], Eckert et al. on ^{144}Nd [41], and by Kohstall et al. on ^{110,112,114,116}Cd [42].

Lacking direct parity measurements in other NRF studies of deformed even–even nuclei, tentative parity assignments were occasionally made based on the observed decay branching ratio R_{expt} from Eq. (7) of a dipole excitation into the lowest to members of the ground-state rotational bands. This was justified for the strongest dipole excitations because all of the 1^+ states where positive parity was measured by Compton polarimetry exhibited branching ratios compatible with $K = 1$. In contrast, all strong $E1$ excitations showed branching ratios compatible with $K = 0$. Some of the assignments of ScM fragments from NRF studies are still based on this procedure. Recent NRF studies with polarized photon beams have confirmed these parity assignments for dipole excitations with large excitation strength [22,43,44]. For weakly dipole excited states, this procedure is, however, not fully justified in general because there occur 1^- states with projection quantum number $K = 1$ and $\Delta K = 0$ $M1$ strength has recently been identified as well [43].

Evolution of $M1$ strength

The ScM occurs in most deformed nuclei, ranging from the pf-shell [45,46] to the heaviest isotopes studied by NRF so far in the Pu isotopic chain [47,48]. Its excitation energy shows some dependence on mass number. It drops from around 4 MeV at mass 50 to below 3 MeV in actinides with weak dependence on the size of the deformation [51,52]. Due to its fragmentation, there exists some ambiguity about what $M1$ strength should be attributed to the ScM [49]. Figure 8 shows a compilation of $M1$ strength attributed to the ScM in even–even rare earth nuclei.

The total strength of the ScM correlates to the square of the nuclear quadrupole deformation parameter [37,53] or, in other words, to the $E2$ excitation strength of the 2_1^+ state [49,54,55]. It is small near shell closures, maximizes at mid-shell and varies smoothly in between. This fact is a clear proof for the collectivity of the low-lying $M1$ strength.

The Scissors Mode in odd-mass nuclei

An appreciable amount of electromagnetic excitation strength in the energy range of the ScM has also been found in odd-A nuclides, too. First data were obtained on ^{163}Dy by the group of Kneissl [56]. Other odd-mass rare earth isotopes were subsequently studied in Stuttgart and in Darmstadt by Kneissl,

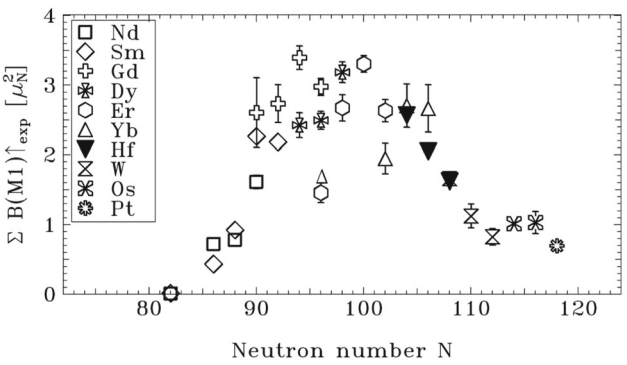

Fig. 8 Systematics of the total $B(M1)\uparrow$ strengths observed in NRF experiments on even–even nuclei as a function of the neutron number (see Refs. [5,49]). The results for the Hf isotopes ^{176,178,180}Hf are shown by filled symbols. *Reprinted with permission from Ref.* [50], *©(2003), by the American Physical Society*

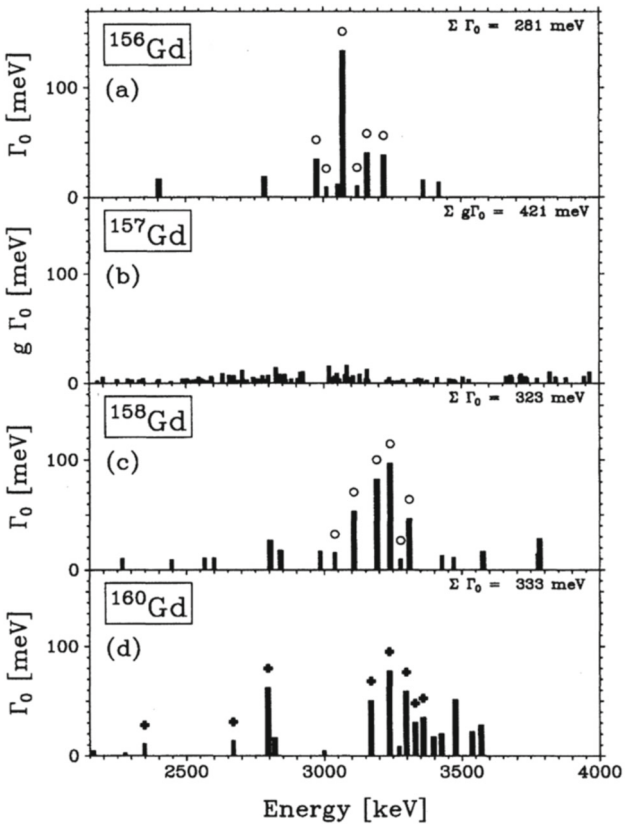

Fig. 9 Dipole strength distributions in the isotopes ^{156,157,158,160}Gd. For the even–even isotopes the ground state widths Γ_0 of $\Delta K = 1$ transitions are plotted. $M1$ character had been measured explicitely for transitions in the even–even isotopes that are marked by symbols. In the case of the odd-mass nucleus ^{157}Gd, because of the unknown spins of the excited states, the products of the ground state decay widths Γ_0 and the spin factor $g = (2J + 1)/(2J_0 + 1)$ (cf. Equation (1)) are plotted. *Reprinted with permission from Ref.* [38], *©(1995), by the American Physical Society*

Richter, and collaborators, e.g. ^{161}Dy [38], ^{155,157}Gd [38,57], ^{159}Tb [57], ^{165}Ho [58,59], ^{169}Tm [58], ^{151,153}Eu [59], and many more.

The interpretation of the data on odd-A is considerably more difficult than for even–even nuclei because the determination of spin and parity quantum numbers and the measurement of the multipolarity of the excitation mode are not practical for odd-mass nuclei in NRF experiments. Moreover, the fragmentation of the ScM in odd-A nuclei is much more pronounced than in their even–even isotopes or isotones leaving the excitation cross section for the individual levels much smaller.

Figure 9 shows a comparison of the strength distribution observed by NRF in some Gadolinium isotopes, including the ^{157}Gd. The larger amount of fragmentation in the latter is apparent. Photoexcitation cross sections in the energy range of the ScM have been measured by now for many stable odd-mass isotopes. A compilation of the data can be found in Refs. [9,14].

Decay pattern of the Scissors Mode

The ScM is an isovector magnetic dipole excitation of the deformed nuclear ground state and it, therefore, decays predominantly via $M1$ transitions into the 0^+_1 and the 2^+_1 states of the ground state rotational band. With decreasing deformation the 1^+ ScM evolves into a two-phonon state of mixed proton-neutron symmetry which can be expected to decay by enhanced $M1$ strength to the excited 0^+_2 state and the 2^+_2 two-phonon states. Such a vibrational pattern has been seen indeed in the classical example of the vibratonal mixed-symmetry multiphonon structure in the nucleus ^{94}Mo [60]. The increased sensitivity to decay transitions in NRF studies with quasi-monochromatic photon beams as compared to those with bremsstrahlung beams or the prolific combination of NRF measurements with γ-ray coincidence studies following β-decay have made the observation of the electromagnetic coupling of the ScM to other intrinsic excitations possible.

Beller et al. [61] observed a decay branch of the main fragment of the ScM of the transitional nucleus ^{154}Gd, its 1^+ state at 2.934 MeV excitation energy, to the first excited 0^+_2 state with an $M1$ branching ratio of $B(M1; 1^+_{2934} \rightarrow 0^+_2)/B(M1; 1^+_{2934} \rightarrow 0^+_1) = 0.06(1)$. This is significant because it required updated calculations for the structure of this nucleus including the prediction for the $\beta\beta$-decay matrix element to ^{154}Sm. A similar situation was previously encountered in ^{98,100}Mo isotopes where, however, definite parity quantum number assignments were lacking [62] and conclusions on the $\beta\beta$-decay matrix element were not drawn.

Very recently, Kleemann et al. [63] studied the $N = 90$ isotone, ^{150}Nd, in an NRF experiment at HIγS. They managed to observe decay transitions of the 1^+ state at 2.994 MeV, the main fragment of the ScM of this nucleus to the band heads of the β- and γ-vibrational bands. Parts of the data are shown in Fig. 10. The decays of the ScM to the ground state band, and to the β and γ bands are differently sensitive to the three Majorana parameters of the Interacting Boson Model. From their data, Kleemann et al. were first able to fix these Majorana parameters by the strengths of sensitive F-vector transitions measured experimentally.

Beck et al. [43] have recently studied the decay branches of the ScM of ^{164}Dy. Comparison of the high-precision data to the Alaga-rule expectations from Eq. (8) revealed the amount of K-mixing in the corresponding 1^+ states at excitation energy 3.159 and 3.173 MeV. Using the previously known photon-scattering cross sections (cf. Fig. 7 panel c) enabled them to determine the strength of a K-conserving $M1$ transition. It was found [43] to have a size of

$$B(M1; 0^+_1 \rightarrow 1^+_{K=0}) = 0.008(1)\ \mu^2_N \qquad (14)$$

and is considered the first measurement of a $\Delta K = 0$ $M1$ transition strength in an even–even nucleus.

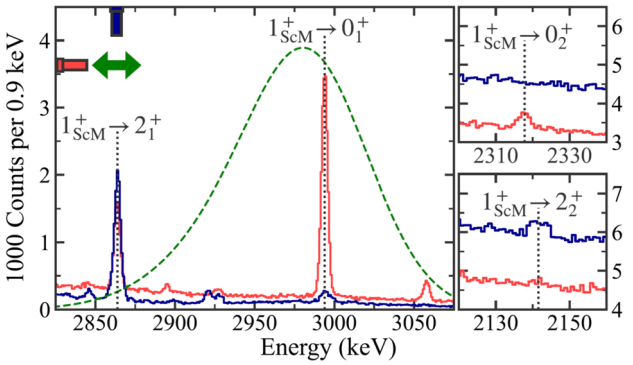

Fig. 10 Three parts of the NRF spectra of ^{150}Nd when irradiated with a 2.98-MeV photon beam. The green dashed line represents the beam's intensity profile. Two HPGe detectors were placed perpendicular to the beam axis. The color-coded azimuthal detector positions are indicated in the top-left schematic along the γ-ray beam's horizontal polarization represented by the green arrow. The 1^+ state of ^{150}Nd at 2.994 MeV excitation energy is the main fragment of the ScM. Its decay transitions to the 0^+_1, 0^+_2, 2^+_1 and 2^+_2 states are labeled correspondingly. The 1^+ state's positive parity is apparent through the pronounced azimuthal asymmetry of its decay transitions to the 0^+ states. *Reprinted with permission from Ref.* [63], *©(2021), by the American Physical Society*

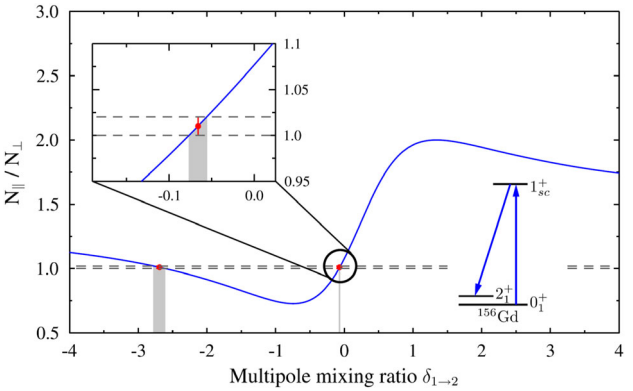

Fig. 11 Measurement of the $E2/M1$ multipole mixing ratio of the $1^+ \to 2^+_1$ transition in ^{156}Gd from the angular distribution of NRF signals in the polarized photon beam at the HIγS facility. The result $\delta = -0.07(1)_{stat}(2)_{syst}$ is shown enlarged in the inlay. Only this solution is consistent with the Alaga rule for the decay branching ratio indicating a small $E2$ contribution to the $1^+ \to 2^+_1$ transition. *Reprinted with permission from Ref.* [22], *©(2017), by the American Physical Society*

Apart from the superior sensitivity to decay branches, NRF studies with polarized quasi-monochromatic photon beams are sensitive to the multipole mixing in the NRF lines, too. Since the ScM originates from the strong nuclear quadrupole deformation it had been an open question for a long time, what its $E2$ decay strength would be. Beck et al. [22] measured the $E2/M1$ multipole mixing ratio of $1^+_{ScM} \to 2^+_1$ transition of the strongest fragment of the ScM of ^{156}Gd. The data are shown in Fig. 11. Similarly, Ide et al. [44] have measured $E2/M1$ multipole mixing ratios of $1^+ \to 2^+_1$ transitions in the transitional nucleus ^{152}Sm. In both cases, the F-vector $E2$ transition strengths from the

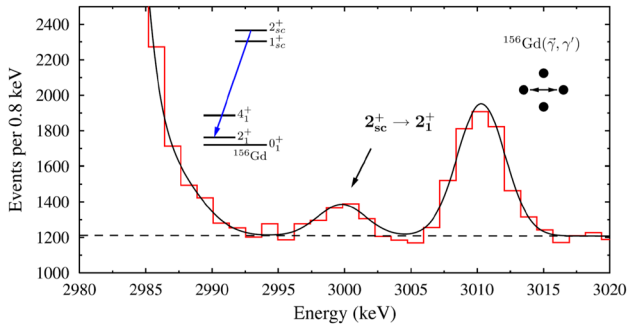

Fig. 12 Candidate for the $2^+_{ScM} \to 2^+_1$ transition in ^{156}Gd at 3.000(1) MeV transition energy. Its intensity and azimuthal asymmetry suggest its interpretation as the decay transition from the 2^+_{ScM} state at 3.089 MeV excitation energy, to the 2^+_1 state at 89 keV. *Reprinted with permission from Ref.* [22], *©(2017), by the American Physical Society*

ScM to the 2^+_1 states are small, of the order of 1 W.u. in ^{152}Sm and even one order of magnitude less in ^{156}Gd which is more rigidly deformed.

Rotational excitation of the Scissors Mode

Corresponding to the F-vector $1^+_{ScM} \to 2^+_1$ $E2$ transition strength between the rotational band built on the 1^+ ScM and the ground state band discussed above, there exists a finite $E2$ excitation strength of the 2^+_{ScM} state belonging to the ScM band. Beck et al. [22] observed evidence for the $E2$ excitation of a 2^+ state of ^{156}Gd at 3.089 MeV excitation energy from the ground state from their NRF experiment at HIγS. The angular distribution of the NRF intensity as shown in Fig. 12 is in agreement with a $0^+_1 \to 2^+ \to 2^+_1$ spin cascade. The corresponding $E2$ excitation strength is compatible with the F-vector $E2$ decay strength of the 1^+ fragment of the ScM at 3.070 MeV. A possible spin staggering in the rotational band built on top of the ScM cannot be excluded. This complication unfortunately prohibits the determination of the still unknown rotational moment of inertia of the scissors mode. Its size remains an open question.

3.2 $E1$ excitations

The $E1$ response of atomic nuclei is dominated by the Giant Dipole Resonance. It peaks at excitation energies between 13 and 26 MeV with a mass dependence of approximately $E(\mathrm{GDR}) \approx 79\, A^{-1/3}$ [1], at least for nuclei with mass numbers exceeding 40. The GDR has an $E1$ decay strength of a few single-particle or Weisskopf units (W.u.). However, it is particle-unbound and, hence, predominantly decays by particle emission, preferentially of neutrons that do not suffer from a Coulomb barrier. The γ decay of the GDR is only known in rare situations and NRF on the GDR has been pioneered only recently.

Since most of the nuclear $E1$ excitation strength is concentrated in the GDR, the strength of particle-bound $E1$ excita-

tion modes is small on a single-particle scale. Comparatively strong $E1$ transitions between low-energy states have transition strength on the order of mW.u. or 10^{-3} e^2fm^2.

A collective source of low-energy $E1$ strength stems from the coupling of the quadrupole with the octupole vibrational degree of freedom. These structures have been systematically studied by NRF measurements. The following subsections address NRF data on vibrational and deformed nuclei. Evidence for particle-core coupling in odd-mass nuclei has been obtained in NRF. We give three examples, from vibrational closed-shell nuclei and from a deformed nucleus. A vast amount of nuclear research in the recent year was devoted to the study and structural clarification of the "low-energy dipole strength", often addressed as "Pygmy Dipole Resonance" (PDR). NRF experiments have contributed very strongly. We restrict us here to a presentation of one example and refer to the literature. Comprehensive review articles on these nuclear structure phenomena exist and are referred to for a deeper study.

3.2.1 Quadrupole-octupole coupled E1 strength

Quadrupole-phonon and octupole phonon excitations belong to the lowest lying collective excitations of the valence shell of heavy vibrational nuclei. For $N = 82$ closed-shell even–even isotones, for instance, a 2^+ state and a 3^- state, both with an excitation strength of about a dozen W.u. from the ground state, are the two lowest-energy excited states. Since particle-hole configurations that generate 2^+ or 3^- states must differ, their coupling may occur. In quadrupole-deformed nuclei, such as many Rare Earth nuclides and Actinides, negative parity bands with enhanced $E3$ excitation strength belong to the lowest-lying bands. NRF experiments have strongly contributed to the data on quadrupole-octupole coupling.

$2^+ \otimes 3^-$ *two-phonon states of vibrational nuclei*

The fundamental isoscalar 2^+ quadrupole-phonon and 3^- octupole phonon excitations of vibrational even–even nuclei may couple to form a quintuplet of states

$$|J\rangle = |2^+ \otimes 3^-\rangle_J \tag{15}$$

with spin quantum numbers $J^\pi = 1^-, 2^-, 3^-, 4^-, 5^-$. Harmonic phonon coupling would result in an excitation energy $E_x(J^\pi) = E(2^+) + E(3^-)$ corresponding to the sum of the energies of the constituent phonons. Deviations from this harmonic limit are expected to arise either from partial blocking effects, which leads to positive anharmonicities increasing the excitation energy, or from "improved self-organization" where the presence of one phonon may result in an energy-optimized modification of the other phonon, which leads to negative anharmonicities. In the harmonic limit, the two-phonon states are uniquely characterized by their defining property that the strength of a single-phonon annihilating transition must be equal to the decay strength of the constituent phonon states, i.e. $B(E2; [2^+ \otimes 3^-]_J \rightarrow 3^-) = B(E2; 2^+ \rightarrow 0_1^+)$ and $B(E3; [2^+ \otimes 3^-]_J \rightarrow 2^+) = B(E3; 3^- \rightarrow 0_1^+)$. The 1^- member of the quadrupole-octupole coupled two-phonon quintuplet can be studied very well with the NRF method. Figures 13 and 21 below show examples for NRF data on quadrupole–octupole coupled two-phonon 1^- states of even–even $N = 82$ isotones and Sn isotopes, respectively. The $E1$ excitation strengths typically amount to a few mW.u. and correlate to the $E1$ strengths between the constituent one-phonon excitations [65] as shown in Fig. 14. More NRF data on two-phonon states can be found, for example, in Refs. [41,66] or in the review article of Ref. [6].

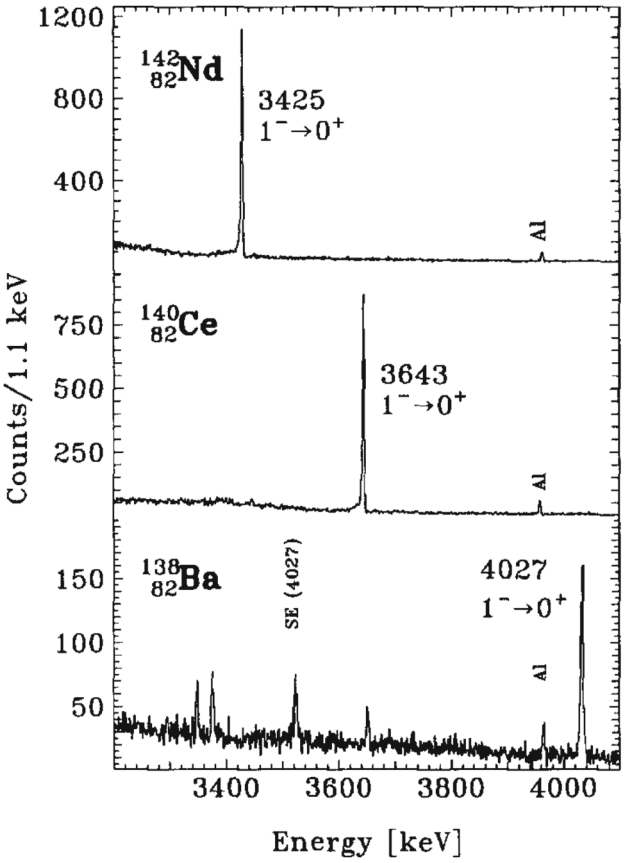

Fig. 13 Photon scattering spectra of the nuclei ^{142}Nd, ^{140}Ce, and ^{138}Ba measured at the Stuttgart Dynamitron accelerator. The iso-lated strong peaks are the $E1$ transitions from the $(2^+ \otimes 3^-)_{1^-}$ states. The lines at 3956 keV stem from the ^{27}Al flux calibra-tion target. *Reprinted from Ref.* [64], *©(1996), with permission from Elsevier*

Quadrupole–octupole coupled E1 strength in deformed nuclei

Octupole vibrations of axially-symmetrically quadrupole-deformed nuclei generate collective rotational bands with projection quantum numbers $K^\pi = 0^-$ to 3^-. The 1_K^- band

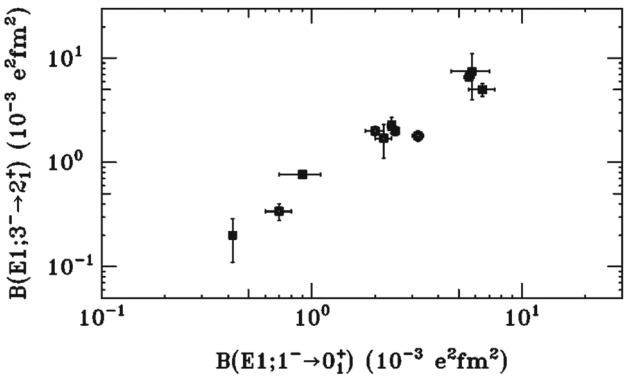

Fig. 14 Comparison of measured low-lying $E1$ transition strengths in vibrators. The scale is chosen as double logarithmic because the $B(E1)$ values cover about two orders of magnitude and their relative errors are comparable in size. There exists a close correlation between the $E1$ transition strengths providing evidence for the quadrupole-octupole-$E1$ collectivity at low energies. *Reprinted with permission from Ref.* [65], *©(1999), by the American Physical Society*

heads of the $K^\pi = 0^-$ and 1^- bands can be studied with NRF.

Comparison of the decay branching ratios to the expectation values from the Alaga rule, Eq. (8) allow for a sensitive and unique assignment of the K quantum numbers as shown in the left panel of Fig. 15. Zilges et al. [68] have provided an overview on low-energy $\Delta K = 0$ $E1$ excitation strengths in selected deformed rare earth nuclei. The data are shown in Fig. 15 on the right. With a typical $E1$ excitation strength of $B(E1; 0_1^+ \rightarrow 1^-) \approx 3$ mW.u., these states display similar strengths as the two-phonon quadrupole-octupole 1^- states observed in spherical nuclei of the same mass region.

When $K^\pi = 0^-$ and 1^- bands are close in energy then their $J^\pi = 1^-$ band heads may mix. The NRF data provide information on the absolute transition matrix elements and, thereby, make the quantitative determination of the mixing matrix element and the ratio Z of the $\Delta K = 1$ to the $\Delta K = 0$ $E1$ matrix elements possible. It is small and amounts to about 10^{-1} to 10^{-2} in some rare earth nuclei [69].

3.2.2 *Particle-core coupled $E1$ excitations*

The preceeding discussion of $E1$ excitations have addressed even–even nuclei. A qualitative difference between NRF research on even–even nuclei and on odd-A nuclei exists because of the much less pronounced angular distributions of NRF intensity for the latter as compared to the former. This fact prevents definitive spin and parity quantum number assignments to the states observed in NRF experiments, except for peculiar situations. Two of these exceptions will be discussed for example in the following paragraphs. The suc-

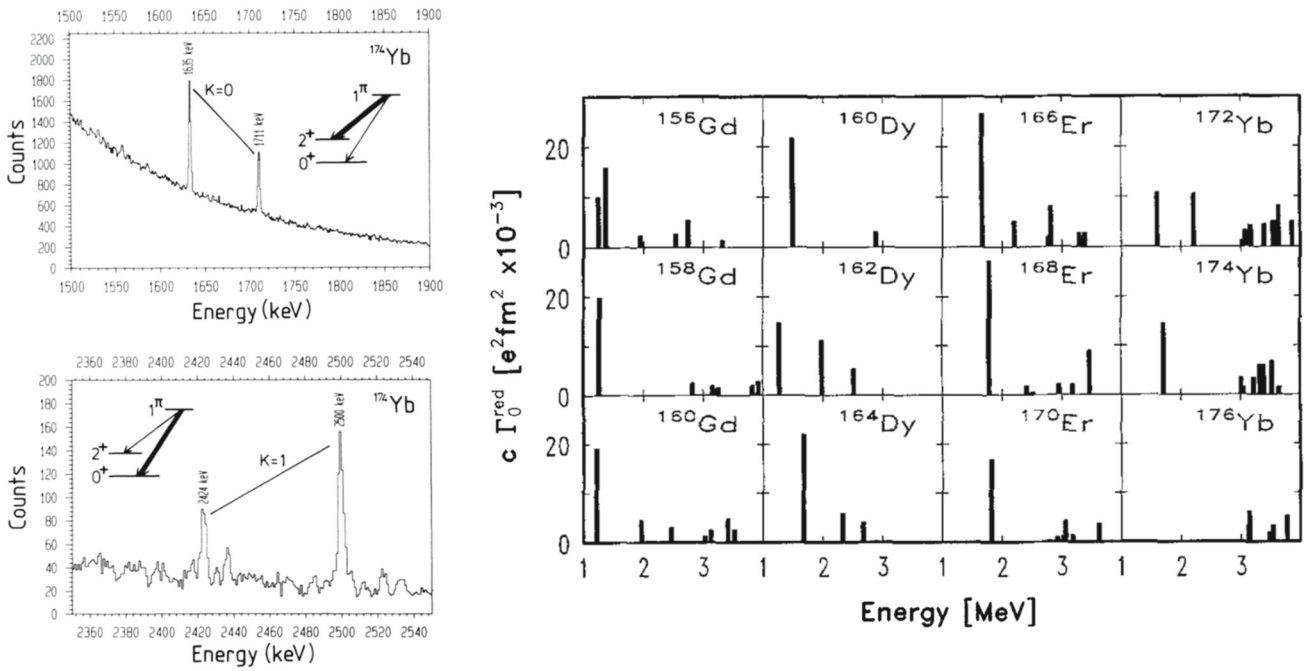

Fig. 15 (Left:) Two parts of an NRF spectrum of ^{174}Yb showing transitions of $J = 1$ states into the ground state band. The ratio of the corresponding peak areas allows for a simple identification of $\Delta K = 0$ and $\Delta K = 1$ transitions in comparison to the Alaga rule, Eqs. (7,8). *Reprinted with permission from Ref.* [67] *©(1990), by the American Physical Society*. (Right:) Distribution of $\Delta K = 0$ dipole strength in the rare earth nuclei ^{156,158,160}Gd, ^{160,162,164}Dy, ^{166,168,170}Er, and ^{172,174,176}Yb, obtained from NRF experiments. In case of negative parity the ordinate value can be identified with the $B(E1) \uparrow$ strength in units of 10^{-3} e^2fm^2. *Reprinted with permission from Ref.* [68]

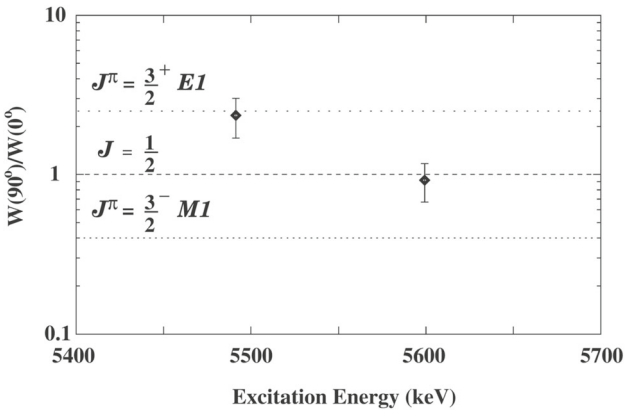

Fig. 16 Azimuthal intensity distribution of the $1/2_1^- \rightarrow J^\pi \rightarrow 1/2_1^-$ NRF signals from dipole excited states of ^{207}Pb at 5.49 MeV and 5.60 MeV excitation energy about the linearly polarized photon beam of the HIγS facility. The horizontal lines mark the ratios for possible spins, $J = 1/2$ or $3/2$, and given polarities. *Reprinted with permission from Ref.* [20]

ceeding paragraph will deal with the phenomenon of particle-core coupled two-phonon states of vibrational nuclei.

Core excitation of ^{207}Pb

Spin and parity quantum number assignments from angular NRF intensity distributions are practically possible if the ground spin quantum number is either $J = 0$ (all even–even nuclei) or $J = 1/2$. In the latter case the NRF intensity distribution for possible dipole excited states with spin and parity quantum numbers $J = 3/2^\pm$ is still sufficiently distinct from the $J = 1/2$ alternative with its exactly isotropic distribution for a $1/2 \rightarrow 1/2 \rightarrow 1/2$ spin sequence. This fact was exploited in a search for the $\nu(3p_{1/2}^{-1})$ neutron hole coupling to the dominant 1^- excitation of ^{208}Pb at 5.5 MeV. The data are displayed in Fig. 16 and allow for a clear identification of the $3/2^+$ level of ^{207}Pb at 5.49 MeV excitation energy [20]. Its $E1$ excitation strength is about a factor of three smaller than the core excitation and indicates clear deviations from the simple weak-coupling limit.

Quasiparticle-octupole coupling in ^{175}Lu As already discussed above, the octupole degree of freedom plays an important role in the low-lying spectrum of heavy nuclei. Coupling a particle to the octupole vibrations with different K quantum numbers results in band structures with similar properties in odd-even and even–even nuclei. Herzberg et al. [70] managed to assign $0^- \otimes 7/2[404]$ structure to the excited $7/2^{(-)}$ and $9/2^{(-)}$ states of the deformed nucleus ^{175}Lu at excitation energies of 1545 and 1611 keV, respectively. The corresponding NRF spectra are displayed in Fig. 17. The unique excitation strengths identify both levels as belonging to the same rotational band. The peculiar branching ratios allow then for a unique $J_K = 7/2_{7/2}$ and $9/2_{7/2}$ spin assignment. Their strengths coincide with the low-energy $E1$ excitation

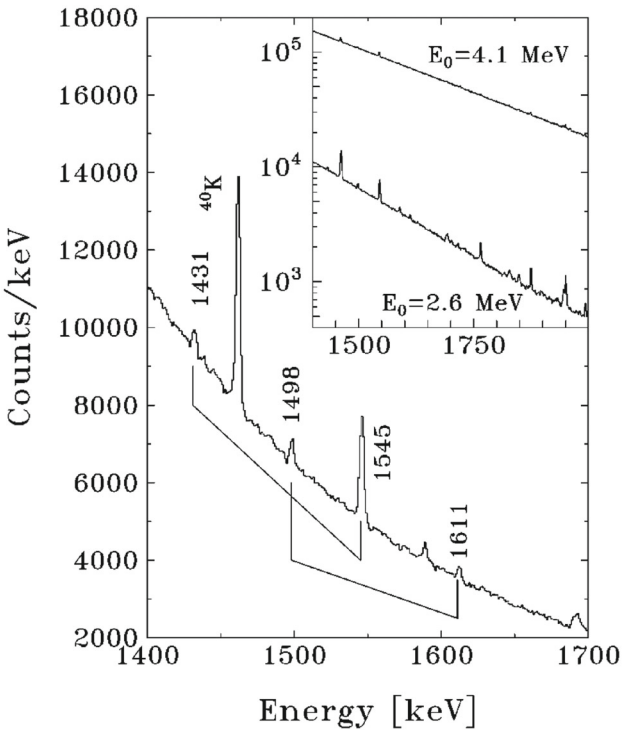

Fig. 17 Part of the NRF spectrum of ^{175}Lu in the energy region of the octupole-vibrational band in the isotone ^{174}Yb. Transitions stemming from the same level are connected by brackets. The peculiar NRF signals and the decay branching ratio make unique spin and K quantum number assignments possible. The inset shows a comparison of the relevant low energy parts of the spectra for two experiments performed at a bremsstrahlung end-point energy of 2.6 MeV (bottom) and 4.1 MeV (top). *Reprinted with permission from Ref.* [70] *©(1997), by the American Physical Society*

strength of the isotone ^{174}Yb (cf. Figure 15) within a factor of two. The $B(E1)$ values for the decay of the octupole vibrational band into the ground state band is expected to be similar in Lu and Yb isotones, if the transitions are considered to predominantly proceed through the collective core deexcitation via the annihilation of the octupole phonon, only, while the odd proton takes the role of a spectator. In addition, the rotational moments of inertia of the octupole vibrational bands in ^{174}Yb and ^{175}Lu are very similar, further supporting their structural assignment.

$2^+ \otimes 3^- \otimes p$ two-phonon states of vibrational nuclei

Evidence for particle-coupling to quadrupole-octupole coupled two-phonon states have also been reported for odd-A vibrational nuclei. Zilges et al. [71] first reported evidence for $2^+ \otimes 3^- \otimes p$ structures in ^{143}Nd where the unpaired neutron occupies the $\nu(2f_{7/2})$ orbital. It can couple with the 1^- core excitation to final spins of $5/2^+$, $7/2^+$ and $9/2^+$. A corresponding NRF spectrum is shown in Fig. 18.

The excitation strength is fragmented. Spin and parity quantum number assignments from NRF intensity distributions are not practical in this case. In the weak-coupling limit,

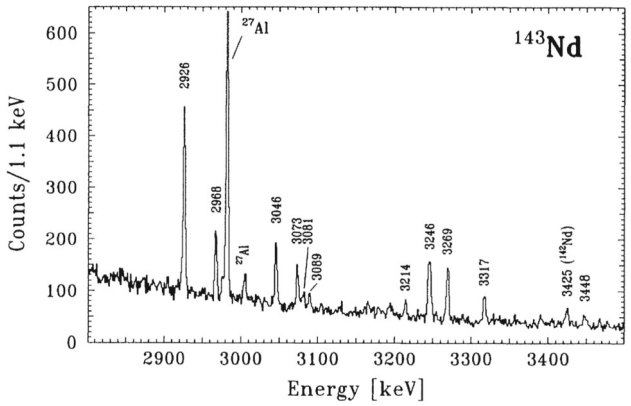

Fig. 18 Part of the NRF spectrum of ^{143}Nd in the energy region of the quadrupole-octupole-coupled 1^- state in the close-shell isotope ^{142}Nd. The NRF lines are interpreted as $E1$ core excitations. *Reprinted with permission from Ref.* [71] *©(1993), by the American Physical Society*

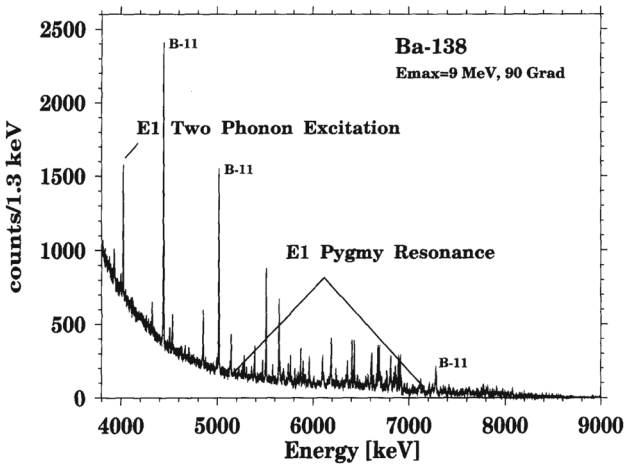

Fig. 19 Photon scattering spectra off ^{138}Ba at the bremsstrahlung beam of the S-DALINAC at Darmstadt. A clear concentration of dipole strength is observed at 5–7.5 MeV. *Reprinted from Ref.* [77], *©(2000), with permission from Elsevier*

the total decay strength from each spin value would correspond to the $E1$ decay strength of the core. In fact, the total observed decay strength amounts to almost three times the $E1$ decay strength of the $2^+ \otimes 3^-$ state of ^{142}Nd (cf. Figure 13). Similar evidence for other $2^+ \otimes 3^- \otimes p$ structures have lateron been identified in a variety of other isotopes, too, see for example Refs. [72–74]

3.2.3 *Pygmy dipole resonance*

An accumulation of $E1$ strength is systematically observed in heavy nuclei riding on the low-energy tail of the GDR. It is often dubbed "Pygmy Dipole Resonance" (PDR) and typically exhausts a few percent of the energy-weighted $E1$ sum rule. The high-resolution investigation of the PDR started at the S-DALINAC [75–78]. Figure 19 shows an early example of the NRF data with unpolarized bremsstrahlung at the improved NRF set-up at the S-DALINAC.

Subsequent studies with polarized photon beams at HIγS established unambigously negative parity of these dipole excitations [16,79] The PDR has attracted a great deal of attention in the last two decades. An appropriate coverage of the material is beyond the scope of this article. Comprehensive review articles on the low-energy dipole strength, e.g. Ref. [15,80], are available for further reading.

3.2.4 *Internal decay of the GDR*

As mentioned above, the GDR dominates the nuclear dipole response, but it predominantly decays by particle emission. Its γ decay into the ground state rotational band of a deformed nucleus has been unknown until recently. Kleemann et al. have succeeded in observing NRF signals from the spherical nuclide ^{140}Ce and from the deformed nuclide ^{154}Sm at 5 different excitation energies between 11 and 18 MeV [81] at HIγS. The data were obtained with linearly and circularly polarized incident photon beams. They allow for an unambiguous determination of the γ-decay branching ratio of the GDR of ^{154}Sm at all probed excitation energies covering both, its $K = 0$ and its $K = 1$ hump. A part of the NRF data and an initial state of the ongoing analysis is shown in Fig. 20. This pioneering experiment has the potential for opening up an entire new route for quantitative studies of the nuclear GDR.

3.3 $E2$ excitations

This subsection will be restricted to the discussion of NRF on even–even nuclei. The $E2$ excitation strength of even–even nuclei is typically concentrated to more than 90% in its 2_1^+ state, except for rare cases at shell closures or for peculiar shape coexistence situations at shape-phase transitional points [82]. This fact is a well known consequence of the attractive proton-neutron quadrupole–quadrupole interaction and the basis for the Q-phonon scheme [83] for approximate decay relations between low-energy quadrupole-collective states. Apart from precision studies in light or closed-shell nuclei, the 2_1^+ state is usually not studied by the NRF method, because it is typically located at low excitation energies such that the excitation width $\Gamma_0 \propto B(E2; 0_1^+ 2_1^+) \times (E\gamma/\hbar c)^5$, which scales with the excitation energy to the fifth power, is usually small; and so is the NRF cross section. Nevertheless, precision studies of the 2_1^+ states of ^{12}C [84] and Sn isotopes [85] aiming at uncertainties of a few percent or less are underway, partly under development of sophisticated variants of the self-absorption technique applied to quasi-monochromatic beams [86].

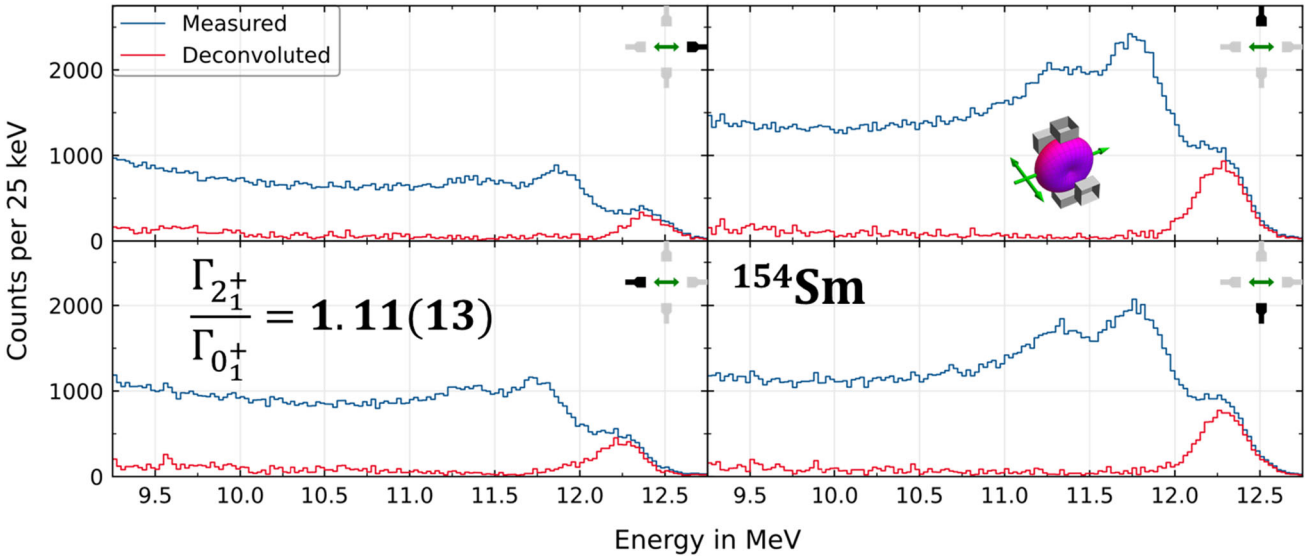

Fig. 20 NRF spectra of a part of the GDR of ^{154}Sm at 12.3 MeV obtained with a quasi-monochromatic, linearly polarized photon beam at HIγS. The raw data measured with four LaBr-detectors at polar angles $\vartheta = 90°$ (the detector arrangement is schematically indicated as an insert in the top right panel) are plotted in blue. Simulated initial NRF intensities compatible with the calibrations and the data are shown in red [81]. The beam polarization and angular NRF intensity distributions allow for the first determination of the γ decay branching ratio of the GDR of ^{154}Sm into its 2_1^+ state and its ground state. A preliminary estimate [81] for the decay branching ratio at 12.3 MeV is indicated in the bottom left panel

In heavy deformed nuclei very little $E2$ excitation strength is observed at energies above 1 or 2 MeV. One exception is the $E2$ strength to the Scissor Mode rotational band which has been discussed above in subsection 3.1.3 because it had completed the discussion on the ScM. In heavy vibrational and transitional nuclei there occurs instead an appreciable amount of $E2$ strength above the 2_1^+ state, which usually is related to strong $M1$ strength to the 2_1^+ state and can be associated with the $2_{1,\mathrm{ms}}^+$ one-quadrupole phonon mixed-symmetry state (MSS). For a review on MSSs the reader is referred to Refs. [13,14]. Since the NRF method has been used to make considerable advances in the research on low-lying $E2$ strength in some closed-shell nuclei and on MSSs, some of these data will be presented here.

Quadrupole excitation strength of semimagic nuclei

The NRF method can be advantageous for the measurement of $E2$ strength for comparatively high-lying excited states as compared to other methods. With increasing excitation energy the level lifetimes drop for a given $B(E2)$ value with the fifth power of the energy. Direct lifetime measurements may then fail for producing precise data when the level lifetimes is below some dozens of fs. Coulomb excitation may suffer from reduced cross section with increasing excitation energy, too.

Bryssinck et al. [87] studied the $E2$ excitation strength of even–even Sn isotopes. Parts of their NRF spectra are displayed in Fig. 21. The $E2$ strength found between 2 and 4 MeV amounts to about 10% of the $B(E2)$ values of the 2_1^+ states and increases with mass number. A variety of 2^+ states of ^{204,206,208}Pb between 3.5 and 7 MeV excitation energy have been studied by Enders et al. [88] using the bremsstrahlung beam at the S-DALINAC accelerator at Darmstadt. Sensitive NRF data on closed-shell Calcium isotopes were provided by Hartmann, Isaak, and Derya et al. [89–91].

Mixed-symmetry phonon excitations

A source of weakly-collective $E2$ excitation strength above the excitation energy of the 2_1^+ state are the isovector quadrupole-phonon valence shell excitations of vibrational nuclei. The description of isovector excitations in the valence shell is possible using a nuclear structure model, which treats the valence space of a heavy nucleus separately with regards to protons and neutrons. Such a model is, e.g., the proton-neutron version of the interacting boson model (IBM-2). Apart from low-lying symmetric states that are multiple isoscalar quadrupole excitations, there exist also eigenstates of the IBM-2 Hamiltonian with wave functions, that are not symmetric with respect to the pairwise exchange of proton and neutron boson labels in the wave functions built from N_π (N_ν) proton (neutron) bosons. These states are called mixed-symmetry states and they correspond to multiple combinations of isoscalar and isovector quadrupole excitations. Formally, the mixed-symmetry states are distinguished from the symmetric ones by the F spin quantum number, which is for bosons the analog of isospin for nucleons. In most practical applications F spin is a rather good quantum num-

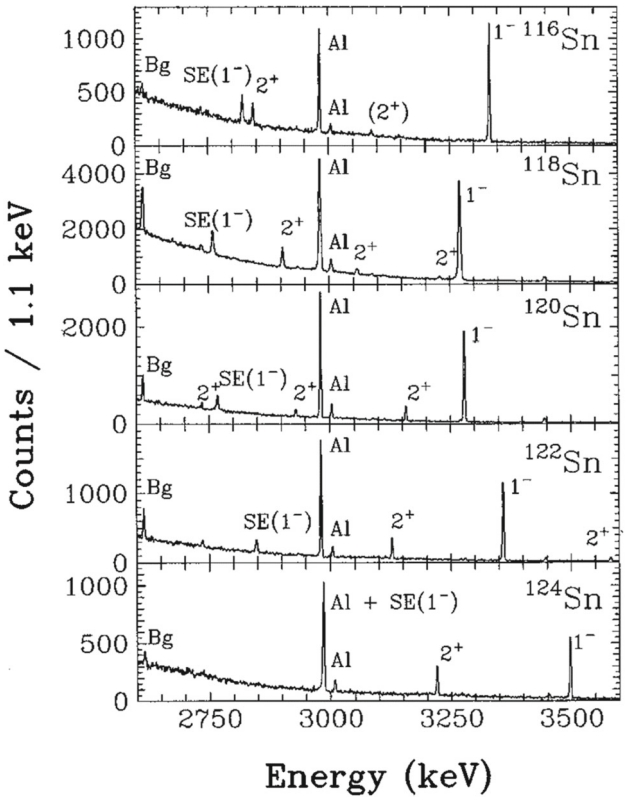

Fig. 21 High energy part (2600 – 3600 keV) of NRF spectra for ^{116,118,120,122,124}Sn from the Stuttgart DYNAMITRON accelerator. The dominating peak in each spectrum corresponds to the deexcitation of the $(2^+ \otimes 3^-)_{1^-}$ state which was discussed above. This peak is indicated with 1^- and its single escape peak with SE(1^-). Prominent 2^+ states are marked with "2^+". The 2614-keV background line from the decay of ^{208}Tl is labeled with "Bg". Lines stemming from the ^{27}Al calibration standard are labeled by "Al". *Reprinted with permission from Ref.* [87] *©(2000), by the American Physical Soci*

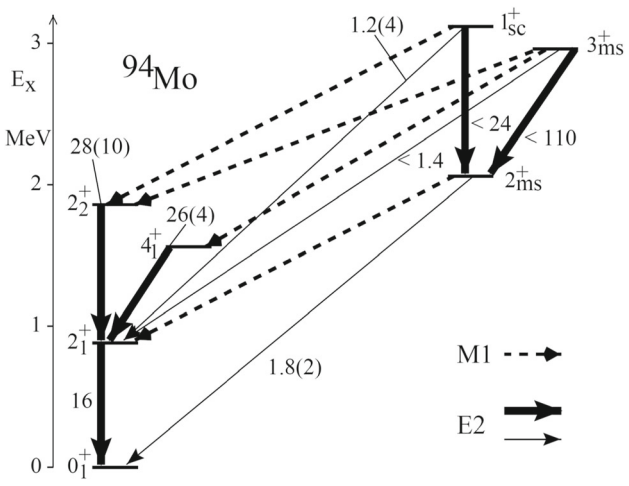

Fig. 22 Partial level scheme of ^{94}Mo. The numbers denote measured $B(E2)$ values in Weisskopf units and $M1$ matrix elements in units of nuclear magnetons. The $1^+, 2^+, 3^+$ levels to the top right decay by large $M1$ matrix elements to the quadrupole-collective symmetric states and form a part of the mixed-symmetry multi-phonon structure of ^{94}Mo. *Reprinted with permission from Ref.* [92] *©(2000), by the American Physical Society*

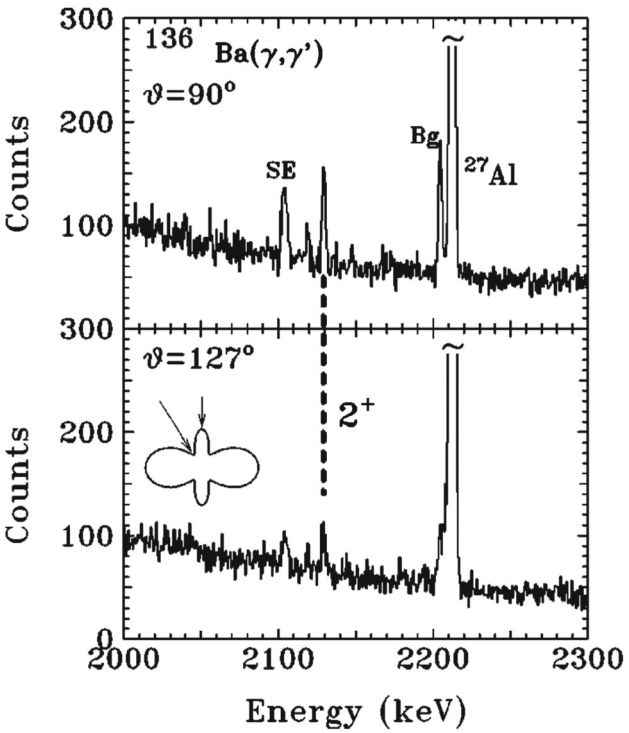

Fig. 23 Part of an NRF spectrum of ^{136}Ba using an incident bremsstrahlung beam with energies $E_\gamma \leq 2.8$ MeV. The angular distribution of the resonant photon scattering intensity observed at 2129 keV clearly indicates the excitation of a 2^+ state. *Reprinted with permission from Ref.* [93] *©(1998), by the American Physical Society*

ber for the low-lying states. While the symmetric states with $F = F_{\max} = (N_\pi + N_\nu)/2$ decay by collective electric quadrupole transitions, the lowest mixed-symmetry states with $F = F_{\max} - 1$ predominantly decay to the symmetric states by magnetic dipole transitions. The best studied mixed-symmetry state is the 1^+ MSS which in deformed nuclei appears as the scissors mode which was discussed in Sect. 3.1.3. Other examples are the isovector quadrupole-phonon excitations of the valence shell of vibrational nuclei. They form multiphonon structures with considerable $M1$ and weakly-collective $E2$ decay strength to the lowest lying, F-symmetric states. Figure 22 shows a part of the multi-phonon MSSs of ^{94}Mo that were partly discovered in NRF experiments.

The historically first $2^+_{1,\mathrm{ms}}$ state which was studied in NRF was the 2^+_4 state of the vibrational nucleus ^{136}Ba at 2.129 MeV excitation energy. Figure 23 shows the relevant parts of the NRF spectrum. The NRF intensity at a polar angle of 90° is about two times of the intensity at 127°. This is proof for the $J = 2$ assignment. The NRF intensity and previously known $M1$ character of the $2^+_4 \to 2^+_1$ transition were the basis for the determination of the signatures of a one-quadrupole phonon MSS, the large $M1$ transition strength

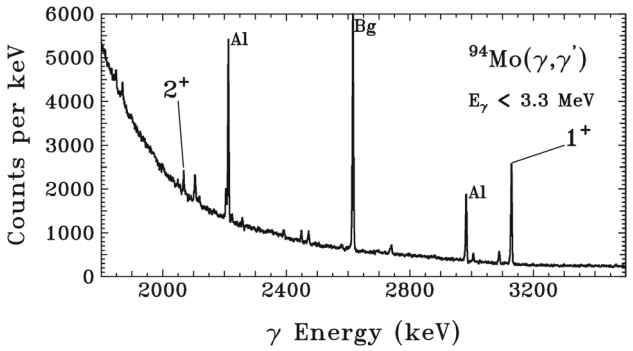

Fig. 24 NRF spectrum of ^{94}Mo displaying the one-quadrupole phonon $2^+_{1,\mathrm{ms}}$ state and the two-phonon $1^+_{1,\mathrm{ms}}$ state. *Reprinted with permission from Ref.* [60] *©(1999), by the American Physical Society*

with a value of $B(M1; 2^+_{1,\mathrm{ms}} \rightarrow 2^+_1) = 0.26(3)\ \mu_N^2$ and the weakly-collective $E2$ decay strength to the ground state [93].

The NRF spectrum of the vibrational nucleus ^{94}Mo is shown in Fig. 24. While the short lifetimes of its low-spin MSSs were determined from NRF, a complementary measurement of their γ-decays was done in $\gamma\gamma$-coincidence spectroscopy following β-decay. This combination of spectroscopic methods provided access to a variety of absolute transition strength that served as the identifying signatures for their solid MS assignments. Further NRF measurements on MSSs were done, for example, in ^{92}Zr by Werner et al. [94] or in ^{148}Sm by Li et al. [95]. A more comprehensive review on experiments on MSSs of vibrational nuclei can be found in Ref. [13].

4 Conclusion

The nuclear spectroscopic method of Nuclear Resonance Fluorescence has made a considerable impact on the advance of knowledge on nuclear low-spin structures. Due to its purely electromagnetic reaction mechanism at the photon point, it provides model-independent, and hence potentially precise and accurate, information on decay transition rates of even highly excited, very short-lived nuclear states. The study of the Scissors Mode starting in the mid-1980s had revived the application of NRF. The advent of intense, fully polarized, quasi-monochromatic, energy tunable, MeV-ranged photon beams, such as at the HIγS facility or planned for ELI-NP have solved the problem of unambiguous parity assignments for a clear identification of the structures under study even at energies where Compton polarimetry is not practical anymore. They boosted the application of the NRF method further since about the turn of the century, for instance for the study of the nuclear Pygmy Dipole Resonance, the scissor mode, spin-flip distributions, or average nuclear properties, such as level densities or γ-ray strength functions. Improved detection capabilities and increasing intensity of the available photon sources continue to inspire nuclear spectroscopists to the development of new and sophisticated methods based on the NRF phenomenon. I am, therefore, convinced that the NRF method will continue to play a very important role for the study of nuclear structure with photons.

Acknowledgements I am grateful to my teachers Peter von Brentano and Ulli Kneissl who have eminently contributed to the development of the field and guided my path to photonuclear reactions. I thank Andreas Zilges and Calin Ur for having encouraged me to the challenge for writing this highly length-limited overview article on a selection of successful NRF studies of nuclear structure phenomena. Many scientists have contributed to the research reviewed in it. I thank all those with whom I could collaborate on NRF research. In particular, I thank Volker Werner and Johann Isaak for efficiently managing our "NRF Group" at Darmstadt, Jörn Kleemann for providing me with material prior to publication, Maike Beuschlein for help on Fig. 1, and Valeriia Skibina for assistance on the manuscript. I thankfully acknowledge the long standing financial support of the German Research Council, DFG, and of the State of Hesse. Both support our efforts for answering ever new research questions exploiting the NRF method, e.g. recently under Grant Nos. SFB 1245 (279384907), GRK 2891 "Nuclear Photonics" (Project ID 499256822), and in the Hessian cluster project ELEMENTS (Project ID 500/10.006).

Funding Open Access funding enabled and organized by Projekt DEAL.

Data Availability Statement This manuscript has no associated data or the data will not be deposited. [Authors' comment: This article is a review of previously and elsewhere published data that can be found in the cited references.]

References

1. A. Bohr, B.R. Mottelson, *Nuclear Structure* (World Scientific, Singapore, 1998)
2. F.R. Metzger, Prog. Nucl. Phys. **7**, 53 (1959)
3. B.L. Berman, S.C. Fultz, Rev. Mod. Phys. **47**, 713 (1975)
4. U.E.P. Berg, U. Kneissl, Annu. Rev. Nucl. Part. Sci. **37**, 33 (1987)
5. U. Kneissl, H.H. Pitz, A. Zilges, Prog. Part. Nucl. Phys. **37**, 349 (1996)
6. U. Kneissl, N. Pietralla, A. Zilges, J. Phys. G **32**, R217 (2006)
7. H.R. Weller, M.W. Ahmed, H. Gao, W. Tornow, Y.K. Wu, M. Gai, R. Miskimen, Prog. Part. Nucl. Phys. **62**, 257 (2009)
8. N. Pietralla, J. Isaak, V. Werner, Eur. Phys. J. A **55**, 237 (2019)
9. A. Zilges, D.L. Balabanski, J. Isaak, N. Pietralla, Prog. Part. Nucl. Phys. **122**, 103903 (2022)

10. U. Kneissl, Prog. Part. Nucl. Phys. **24**, 41 (1990)
11. A. Richter, Prog. Part. Nucl. Phys. **34**, 261 (1995)
12. D. Zawischa, J. Phys. G **24**, 683 (1998)
13. N. Pietralla, P. von Brentano, A. Lisetskiy, Prog. Part. Nucl. Phys. **60**, 225 (2008)
14. K. Heyde, P. von Neumann-Cosel, A. Richter, Rev. Mod. Phys. **82**, 2365–2419 (2010)
15. D. Savran, T. Aumann, A. Zilges, Prog. Part. Nucl. Phys. **70**, 210 (2013)
16. N. Pietralla, Z. Berant, V.N. Litvinenko, S. Hartman, F.F. Mikhailov, I.V. Pinayev, G. Swift, M.W. Ahmed, J.H. Kelley, S.O. Nelson, R. Prior, K. Sabourov, A.P. Tonchev, H.R. Weller, Phys. Rev. Lett. **88**, 012502 (2002)
17. N. Pietralla, H.R. Weller, V.N. Litvinenko, M.W. Ahmed, A.P. Tonchev, Nucl. Instr. Methods Phys. Res. A **483**, 556 (2002)
18. N. Pietralla, M.W. Ahmed, C. Fransen, V.N. Litvinenko, A.P. Tonchev, H.R. Weller, A.I.P. Conf. Proc. **656**, 365 (2003)
19. C. Iliadis, U. Friman-Gayer, Eur. Phys. J. A **57**, 190 (2021)
20. N. Pietralla, T. Li, M. Fritzsche, M. Ahmed, T. Ahn, A. Costin, J. Enders, J. Li, S. Müller, P. von Neumann-Cosel, I. Pinayev, V. Ponomarev, D. Savran, A. Tonchev, W. Tornow, H. Weller, V. Werner, Y. Wu, A. Zilges, Phys. Lett. B **681**, 134 (2009)
21. K. Krane, R. Steffen, R. Wheeler, Atom. Data Nucl. Data Tables **11**, 351 (1973)
22. T. Beck, J. Beller, N. Pietralla, M. Bhike, J. Birkhan, V. Derya, U. Gayer, A. Hennig, J. Isaak, B. Löher, V.Y. Ponomarev, A. Richter, C. Romig, D. Savran, M. Scheck, W. Tornow, V. Werner, A. Zilges, M. Zweidinger, Phys. Rev. Lett. **118**, 212502 (2017)
23. G. Alaga, K. Alder, A. Bohr, B.R. Mottelson, K. Dan, Vidensk. Selesk. Mat. Fys. Medd. **29**, 1 (1955)
24. A.F. Lisetskiy, R.V. Jolos, N. Pietralla, P. von Brentano, Phys. Rev. C **60**, 064310 (1999)
25. U. Friman-Gayer, C. Romig, T. Hüther, K. Albe, S. Bacca, T. Beck, M. Berger, J. Birkhan, K. Hebeler, O.J. Hernandez, J. Isaak, S. König, N. Pietralla, P.C. Ries, J. Rohrer, R. Roth, D. Savran, M. Scheck, A. Schwenk, R. Seutin, V. Werner, Phys. Rev. Lett. **126**, 102501 (2021)
26. T.C. Li, N. Pietralla, A.P. Tonchev, M.W. Ahmed, T. Ahn, C. Angell, M.A. Blackston, A. Costin, K.J. Keeter, J. Li, A. Lisetskiy, S. Mikhailov, Y. Parpottas, B.A. Perdue, G. Rainovski, W. Tornow, H.R. Weller, Y.K. Wu, Phys. Rev. C **73**, 054306 (2006)
27. U. Gayer, T. Beck, M. Bhike, J. Isaak, N. Pietralla, P.C. Ries, D. Savran, M. Schilling, W. Tornow, V. Werner, Phys. Rev. C **100**, 034305 (2019)
28. W. Tornow, A.P. Tonchev, S.W. Finch, Krishichayan, X.B. Wang, A.C. Hayes, H.G.D. Yeomans, D.A. Newmark, Phys. Lett. B **835**, 137576 (2022)
29. D. Bohle, A. Richter, W. Steffen, A.E.L. Dieperink, N.L. Iudice, F. Palumbo, O. Scholten, Phys. Lett. B **137**, 27 (1984)
30. U.E.P. Berg, C. Bläsing, J. Drexler, R.D. Heil, U. Kneissl, W. Naatz, R. Ratzek, S. Schennach, R. Stock, T. Weber, H. Wickert, B. Fischer, H. Hollick, D. Kollewe, Phys. Lett. **149B**, 59 (1984)
31. D. Bohle, A. Richter, U. Berg, J. Drexler, R. Heil, U. Kneissl, H. Metzger, R. Stock, B. Fischer, H. Hollick, D. Kollewe, Nucl. Phys. **458**, 205 (1986)
32. C. Wesselborg, P. von Brentano, K.O. Zell, R.D. Heil, H.H. Pitz, U.E.P. Berg, U. Kneissl, S. Lindenstruth, U. Seemann, R. Stock, Phys. Lett. B **207**, 22 (1988)
33. B. Kasten, R.D. Heil, P.V. Brentano, P.A. Butler, S.D. Hoblit, U. Kneissl, S. Lindenstruth, G. Muller, H.H. Pitz, K.W. Rose, W. Scharfe, M. Schumacher, U. Seemann, Th. Weber, C. Wesselborg, A. Zilges, Phys. Rev. Lett. **63**, 609 (1989). (**Erratum ibid 2695**)
34. R.D. Heil, B. Kasten, W. Scharfe, P.A. Butler, H. Friedrichs, S.D. Hoblit, U. Kneissl, S. Lindenstruth, M. Ludwig, G. Muller, H.H. Pitz, K.W. Rose, M. Schumacher, U. Seemann, J. Simpson, P. von Brentano, Th. Weber, C. Wesselborg, A. Zilges, Nucl. Phys. A **506**, 223 (1990)
35. H. Friedrichs, B. Schlitt, J. Margraf, S. Lindenstruth, C. Wesselborg, R.D. Heil, H.H. Pitz, U. Kneissl, P. von Brentano, R.D. Herzberg, A. Zilges, D. Hager, G. Muller, M. Schumacher, Phys. Rev. C **45**, R892 (1992)
36. H. Friedrichs, D. Hager, P. von Brentano, R.D. Heil, R.-D. Herzberg, U. Kneissl, J. Margraf, G. Muller, H.H. Pitz, B. Schlitt, M. Schumacher, C. Wesselborg, A. Zilges, Nucl. Phys. A **567**, 266 (1994)
37. J. Margraf, R.D. Heil, U. Kneissl, U. Maier, H.H. Pitz, H. Friedrichs, S. Lindenstruth, B. Schlitt, C. Wesselborg, P. von Brentano, R.-D. Herzberg, A. Zilges, Phys. Rev. C **47**, 1474 (1993)
38. J. Margraf, T. Eckert, M. Rittner, I. Bauske, O. Beck, U. Kneissl, H. Maser, H.H. Pitz, A. Schiller, P. von Brentano, R. Fischer, R.-D. Herzberg, N. Pietralla, A. Zilges, H. Friedrichs, Phys. Rev. C **52**, 2429 (1995)
39. H. Maser, N. Pietralla, P. von Brentano, R.-D. Herzberg, U. Kneissl, J. Margraf, H.H. Pitz, A. Zilges, Phys. Rev. C **54**, R2129 (1996)
40. H. Maser, S. Lindenstruth, I. Bauske, O. Beck, P. von Brentano, T. Eckert, H. Friedrichs, R.D. Heil, R.-D. Herzberg, A. Jung, U. Kneissl, J. Margraf, N. Pietralla, H.H. Pitz, C. Wesselborg, A. Zilges, Phys. Rev. C **53**, 2749 (1996)
41. T. Eckert, O. Beck, J. Besserer, P. von Brentano, R. Fischer, R.-D. Herzberg, U. Kneissl, J. Margraf, H. Maser, A. Nord, N. Pietralla, H.H. Pitz, S.W. Yates, A. Zilges, Phys. Rev. C56 (1997) 1256; Erratum C57 (1998) 1007
42. C. Kohstall, D. Belic, P. von Brentano, C. Fransen, A. Gade, R.-D. Herzberg, J. Jolie, U. Kneissl, A. Linnemann, A. Nord, N. Pietralla, H.H. Pitz, M. Scheck, F. Stedile, V. Werner, S.W. Yates, Phys. Rev. C **72**, 034302 (2005)
43. T. Beck, V. Werner, N. Pietralla, M. Bhike, N. Cooper, U. Friman-Gayer, J. Isaak, R.V. Jolos, J. Kleemann, Krishichayan, O. Papst, W. Tornow, C. Bernards, B.P. Crider, R.S. Ilieva, B. Löher, C. Mihai, F. Naqvi, S. Pascu, E.E. Peters, F.M. Prados-Estevez, T.J. Ross, D. Savran, J.R. Vanhoy, A. Zilges, Phys. Rev. Lett. **125**, 092501 (2020)
44. K.E. Ide, T. Beck, V. Werner, M. Berger, S.W. Finch, U. Friman-Gayer, J. Kleemann, Krishichayan, B. Löher, O. Papst, N. Pietralla, D. Savran, W. Tornow, M. Weinert, J. Wiederhold, A. Zilges, Phys. Rev. C **103**, 054302 (2021)
45. A. Richter, Nucl. Phys. A **507**, 99c (1990)
46. H. Pai, J. Beller, N. Benouaret, J. Enders, T. Hartmann, O. Karg, P. von Neumann-Cosel, N. Pietralla, V.Y. Ponomarev, C. Romig, M. Scheck, L. Schnorrenberger, S. Volz, M. Zweidinger, Phys. Rev. C **88**, 054316 (2013)
47. W. Bertozzi, J.A. Caggiano, W.K. Hensley, M.S. Johnson, S.E. Korbly, R.J. Ledoux, D.P. McNabb, E.B. Norman, W.H. Park, G.A. Warren, Phys. Rev. C **78**, 041601 (2008)
48. B.J. Quiter, T. Laplace, B.A. Ludewigt, S.D. Ambers, B.L. Goldblum, S. Korbly, C. Hicks, C. Wilson, Phys. Rev. C **86**, 034307 (2012)
49. N. Pietralla, P. von Brentano, R.-D. Herzberg, U. Kneissl, J. Margraf, H. Maser, H.H. Pitz, A. Zilges, Phys. Rev. C **52**, R2317 (1995)
50. M. Scheck, D. Belic, P. von Brentano, J.J. Carroll, C. Fransen, A. Gade, H. von Garrel, U. Kneissl, C. Kohlstall, A. Linnemann, N. Pietralla, H.H. Pitz, F. Stedile, R. Toman, V. Werner, PRC **67**, 064313 (2003)
51. N. Pietralla, P. von Brentano, R.-D. Herzberg, U. Kneissl, N. Lo Iudice, H. Maser, H.H. Pitz, A. Zilges, Phys. Rev. C **58**, 184 (1998)
52. J. Enders, H. Kaiser, H.P. von Neumann-Cosel, C. Rangacharyulu, A. Richter, Phys. Rev. **C59**, R1851 (1999)
53. W. Ziegler, C. Rangacharyulu, A. Richter, C. Spieler, Phys. Rev. Lett. **65**, 2515 (1990)
54. C. Rangacharyulu, A. Richter, H.J. Wörtche, W. Ziegler, R.F. Casten, Phys. Rev. C **43**, R949 (1991)

55. P. von Neumann-Cosel, J.N. Ginocchio, H. Bauer, A. Richter, Phys. Rev. Lett. **75**, 4178 (1995)
56. I. Bauske, J.M. Arias, P. von Brentano, A. Frank, H. Friedrichs, R.D. Heil, R.-O. Herzberg, F. Hoyler, P. Van lsacker, U. Kneissl, J. Margraf, H.H. Pitz, C. Wesselborg, A. Zilges, Phys. Rev. Lett. **71**, 975–978 (1993)
57. A. Nord, A. Schiller, T. Eckert, O. Beck, J. Besserer, P. von Brentano, R. Fischer, R.-D. Herzberg, D. Jäger, U. Kneissl, J. Margraf, H. Maser, N. Pietralla, H.H. Pitz, M. Rittner, A. Zilges, Phys. Rev. C **54**, 2287 (1996)
58. A. Huxel, P. von Brentano, J. Eberth, J. Enders, R.-D. Herzberg, P. von Neumann-Cosel, N. Nicolay, N. Pietralla, H. Prade, C. Rangacharyulu, J. Reif, A. Richter, C. Schlegel, R. Schwengner, S. Skoda, H.G. Thomas, I. Wiedenhöver, G. Winter, A. Zilges, Nucl. Phys. A **645**, 239 (1999)
59. A. Nord, J. Enders, A.E. de Almeida Pinto, D. Belic, P. von Brentano, C. Fransen, U. Kneissl, C. Kohstall, A. Linnemann, P. von Neumann-Cosel, N. Pietralla, H.H. Pitz, A. Richter, F. Stedile, V. Werner, Phys. Rev. C **67**, 034307 (2003)
60. N. Pietralla, C. Fransen, D. Belic, P. von Brentano, C. Frießner, U. Kneissl, A. Linnemann, A. Nord, H.H. Pitz, T. Otsuka, I. Schneider, V. Werner, I. Wiedenhöver, Phys. Rev. Lett. **83**, 1303 (1999)
61. J. Beller, N. Pietralla, J. Barea, M. Elvers, J. Endres, C. Fransen, J. Kotila, O. Möller, A. Richter, T.R. Rodríguez, C. Romig, D. Savran, M. Scheck, L. Schnorrenberger, K. Sonnabend, V. Werner, A. Zilges, M. Zweidinger, Phys. Rev. Lett. **111**, 172501 (2013)
62. G. Rusev, R. Schwengner, F. Dönau, S. Frauendorf, L. Käubler, L.K. Kostov, S. Mallion, K.D. Schilling, A. Wagner, E. Grosse, H. von Garrel, U. Kneißl, C. Kohstall, M. Kreutz, H.H. Pitz, M. Scheck, F. Stedile, P. von Brentano, J. Jolie, A. Linnemann, N. Pietralla, V. Werner, Phys. Rev. Lett. **95**, 062501 (2005)
63. J. Kleemann, T. Beck, U. Friman-Gayer, N. Pietralla, V. Werner, S.W. Finch, J. Kotila, Krishichayan, B. Löher, H. Pai, O. Papst, W. Tornow, M. Weinert, A. Zilges, Phys. Rev. C **104**, L061302 (2021)
64. A. Zilges, P. von Brentano, R.-D. Herzberg, U. Kneissl, J. Margraf, H.H. Pitz, Nucl. Phys. A **599**, 147c (1996)
65. N. Pietralla, Phys. Rev. C **59**, 2941 (1999)
66. H. von Garrel, P. von Brentano, C. Fransen, G. Friessner, N. Hollmann, J. Jolie, F. Käppeler, L. Käubler, U. Kneissl, C. Kohstall, L. Kostov, A. Linnemann, D. Mücher, N. Pietralla, H.H. Pitz, G. Rusev, M. Scheck, K.D. Schilling, C. Scholl, R. Schwengner, F. Stedile, S. Walter, V. Werner, K. Wisshak, Phys. Rev. C **73**, 054315 (2006)
67. A. Zilges, P. von Brentano, A. Richter, R.D. Heil, U. Kneissl, H.H. Pitz, C. Wesselborg, Phys. Rev. C **42**, 1945 (1990)
68. A. Zilges, P. von Brentano, H. Friedrichs, R.D. Heil, U. Kneissl, S. Lindenstruth, H.H. Pitz, C. Wesselborg, Z. Phys. A **340**, 155 (1991)
69. P. von Brentano, N.V. Zamfir, A. Zilges, Phys. Lett. **278B**, 221 (1992)
70. R.-D. Herzberg, C. Fransen, R. Fischer, O. Beck, D. Belic, J. Besserer, P. von Brentano, T. Eckert, U. Kneissl, B. Krischok, J. Margraf, H. Maser, A. Nord, N. Pietralla, H.H. Pitz, A. Wolpert, A. Zilges, Phys. Rev. C **56**, 2484 (1997)
71. A. Zilges, R.-D. Herzberg, P. von Brentano, F. Dönau, R.D. Heil, R.V. Jolos, U. Kneissl, J. Margraf, H.H. Pitz, C. Wesselborg, Phys. Rev. Lett. **70**, 2880 (1993)
72. J. Besserer, O. Beck, P. von Brentano, T. Eckert, R.-D. Herzberg, D. Jäger, U. Kneissl, J. Margraf, H. Maser, A. Nord, N. Pietralla, H.H. Pitz, A. Zilges, Phys. Rev. C **56**, 1276 (1997)
73. M. Scheck, H. von Garrel, N. Tsoneva, D. Belic, P. von Brentano, C. Fransen, A. Gade, J. Jolie, U. Kneissl, C. Kohstall, A. Linnemann, A. Nord, N. Pietralla, H.H. Pitz, F. Stedile, C. Stoyanov, V. Werner, Phys. Rev. C **70**, 044319 (2004)
74. M. Scheck, P.V. Brentano, C. Fransen, U. Kneissl, C. Kohstall, A. Linnemann, D. Mücher, N. Pietralla, H.H. Pitz, C. Scholl, F. Stedile, S. Walter, V. Werner, S.W. Yates, Phys. Rev. C **75**, 044313 (2007)
75. R.-D. Herzberg, P. von Brentano, J. Eberth, J. Enders, R. Fischer, N. Huxel, T. Klemme, P. von Neumann-Cosel, N. Nicolay, N. Pietralla, V.Y. Ponomarev, J. Reif, A. Richter, C. Schlegel, R. Schwengner, S. Skoda, H.G. Thomas, I. Wiedenhöver, G. Winter, A. Zilges, Phys. Lett. B **390**, 49 (1997)
76. R.-D. Herzberg, C. Fransen, P. von Brentano, J. Eberth, J. Enders, A. Fitzler, L. Käubler, H. Kaiser, P. von Neumann-Cosel, N. Pietralla, VYu. Ponomarev, H. Prade, A. Richter, H. Schnare, R. Schwengner, S. Skoda, H.G. Thomas, H. Tiesler, D. Weisshaar, I. Wiedenhöver, Phys. Rev. C **60**, 051307 (1999)
77. A. Zilges, P. Mohr, Prog. Part. Nucl. Phys. **44**, 39 (2000)
78. A. Zilges, S. Volz, M. Babilon, T. Hartmann, P. Mohr, K. Vogt, Phys. Lett. B **542**, 43 (2002)
79. A.P. Tonchev, S.L. Hammond, J.H. Kelley, E. Kwan, H. Lenske, G. Rusev, W. Tornow, N. Tsoneva, Phys. Rev. Lett. **104**, 072501 (2010)
80. A. Bracco, E.G. Lanza, A. Tamii, Prog. Part. Nucl. Phys. **106**, 360 (2019)
81. J. Kleemann, private communication
82. W. Witt, V. Werner, N. Pietralla, M. Albers, A.D. Ayangeakaa, B. Bucher, M.P. Carpenter, D. Cline, H.M. David, A. Hayes, C. Hoffman, R.V.F. Janssens, B.P. Kay, F.G. Kondev, W. Korten, T. Lauritsen, O. Möller, G. Rainovski, G. Savard, D. Seweryniak, J. Smith, R. Stegmann, S. Zhu, C.Y. Wu, Phys. Rev. C **98**, 041302(R) (2018)
83. N. Pietralla, P. von Brentano, R.F. Casten, T. Otsuka, N.V. Zamfir, Phys. Rev. Lett. **73**, 2962 (1994)
84. J. Isaak, private communication
85. M. Beuschlein, private communication
86. D. Savran, J. Isaak, Nucl. Instrum. Methods Phys. Res. A **899**, 111 (2018)
87. J. Bryssinck, L. Govor, VYu. Ponomarev, F. Bauwens, O. Beck, D. Belic, P. von Brentano, D. De Frenne, T. Eckert, C. Fransen, K. Govaert, R.-D. Herzberg, E. Jacobs, U. Kneissl, H. Maser, A. Nord, N. Pietralla, H.H. Pitz, V. Werner, Phys. Rev. C **61**, 024309 (2000)
88. J. Enders, P. von Brentano, J. Eberth, A. Fitzler, C. Fransen, R.-D. Herzberg, H. Kaiser, L. Käubler, P. von Neumann-Cosel, N. Pietralla, V.Y. Ponomarev, A. Richter, R.S.I. Wiedenhöver, Nucl. Phys. A **724**, 243 (2003)
89. T. Hartmann, J. Enders, P. Mohr, K. Vogt, S. Volz, A. Zilges, Phys. Rev. C **65**, 034301 (2002)
90. J. Isaak, D. Savran, M. Fritzsche, D. Galaviz, T. Hartmann, S. Kamerdzhiev, J.H. Kelley, E. Kwan, N. Pietralla, C. Romig, G. Rusev, K. Sonnabend, A.P. Tonchev, W. Tornow, A. Zilges, Phys. Rev. C **83**, 034304 (2011)
91. V. Derya, D. Savran, J. Endres, M.N. Harakeh, H. Hergert, J.H. Kelley, P. Papakonstantinou, N. Pietralla, V.Y. Ponomarev, R. Roth, G. Rusev, A.P. Tonchev, W. Tornow, H.J. Wortche, A. Zilges, Phys. Lett. B **730**, 288 (2014)
92. N. Pietralla, C. Fransen, P. von Brentano, A. Dewald, A. Fitzler, C. Frießner, J. Gableske, Phys. Rev. Lett. **84**, 3775 (2000)
93. N. Pietralla, D. Belic, P. von Brentano, C. Fransen, R.-D. Herzberg, U. Kneissl, H. Maser, P. Matschinsky, A. Nord, T. Otsuka, H.H. Pitz, V. Werner, I. Wiedenhöver, Phys. Rev. C **58**, 796 (1998)
94. V. Werner, D. Belic, P. von Brentano, C. Fransen, A. Gade, H. von Garrel, J. Jolie, U. Kneissl, C. Kohstall, A. Linnemann, A. Lisetskiy, N. Pietralla, H. Pitz, M. Scheck, K.-H. Speidel, F. Stedile, S. Yates, Phys. Lett. B **550**, 140 (2002)
95. T.C. Li, N. Pietralla, C. Fransen, H.V. Garrel, U. Kneissl, C. Kohstall, A. Linnemann, H.H. Pitz, G. Rainovski, A. Richter, M. Scheck, F. Stedile, P.V. Brentano, P.V. Neumann-Cosel, V. Werner, Phys. Rev. C **71**, 044318 (2005)